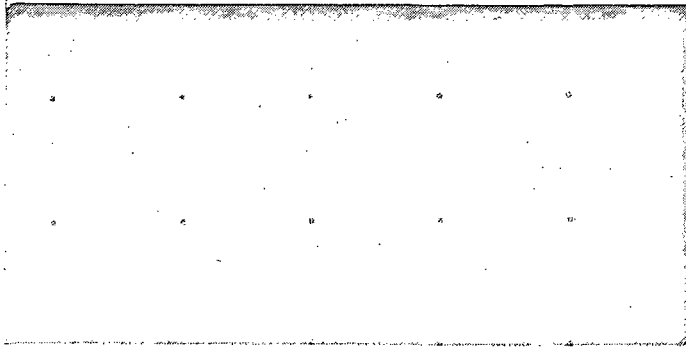


N 12-19867



**CASE FILE
COPY**



Lockheed

HUNTSVILLE RESEARCH & ENGINEERING CENTER

LOCKHEED MISSILES & SPACE COMPANY, INC.
A SUBSIDIARY OF LOCKHEED AIRCRAFT CORPORATION

HUNTSVILLE, ALABAMA

LOCKHEED MISSILES & SPACE COMPANY
HUNTSVILLE RESEARCH & ENGINEERING CENTER
HUNTSVILLE RESEARCH PARK
4800 BRADFORD DRIVE, HUNTSVILLE, ALABAMA

THE APPLICATION OF OPTIMAL
CONTROL TECHNIQUES
TO ADVANCED MANNED MISSIONS

VOLUME I

February 1972

Contract NAS8-25578

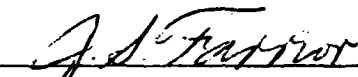
by

C. L. Connor
W. Trautwein

APPROVED:



T. R. Beal, Manager
Dynamics & Guidance Department


J. S. Farrior
Resident Director

FOREWORD

This report presents in two volumes the results of work performed during the period of May 1970 to February 1972 by Lockheed's Huntsville Research & Engineering Center while under contract to the National Aeronautics and Space Administration for the Aero-Astrodynamic Laboratory of Marshall Space Flight Center (MSFC), Contract NAS8-25578.

The report documents the work performed on the "Application of Optimal Techniques to Advanced Manned Missions," namely the composite shuttle ascent phase.

Mr. J. M. Livingston of NASA-MSFC, Aero-Astrodynamic Laboratory, S&E-AERO-DF, was the MSFC Contracting Officer's Representative. Mr. C. L. Connor was the project engineer at Lockheed. Major contributors were Dr. W. Trautwein, who provided technical assistance, and Mr. A. M. Hansing, who performed the hybrid programming. Mr. K. R. Leimbach and Mr. W. G. Green provided assistance in establishing payload sensitivities due to structural loads and trajectory errors, respectively.

CONTENTS

Section		Page
	FOREWORD	ii
	SUMMARY AND INTRODUCTION	iv
1	HYBRID OPTIMIZER PROGRAM	1-1
	1.1 Basic Scheme	1-1
	1.2 Update Interval	1-1
	1.3 Optimization Interval	1-3
	1.4 Grid Search	1-5
	1.5 Reducing the Sensitivity to Parameter Uncertainties	1-7
	1.6 Performance Evaluation	1-7
2	MATHEMATICAL MODELS	2-1
	2.1 Two-Degree-of-Freedom Model	2-1
	2.2 Six-Degree-of-Freedom Model	2-3
	2.3 Synthetic Wind Profiles	2-7
	2.4 Booster/Orbiter Structural Interfacing Loads	2-7
	2.5 Major Payload Sensitivities	2-15
3	OPTIMIZATION RESULTS	3-1
	3.1 Pitch Controller Design for Maximum Load Relief Based on 2-DOF Model	3-1
	3.2 Pitch Controller Design for Maximum Load Relief Based on 6-DOF Model	3-5
	3.3 Yaw Controller Design for Maximum Load Relief	3-9
	3.4 Pitch Controller Design for Maximum Payload	3-9
	3.5 Yaw Controller Design for Maximum Payload	3-20
	3.6 Effects of Wind Uncertainties on the Optimized Control System	3-25
4	CONCLUSIONS AND RECOMMENDATIONS	4-1
5	REFERENCES	5-1

SUMMARY AND INTRODUCTION

The work reported here is concerned with two problems in the area of optimal control and its application to the design of attitude control systems for advanced complex aerospace vehicles:

- Specification of performance criteria in terms of structural load minimization and/or maximum orbital payload injection requirements of the controlled vehicle.
- Formulation (and solution) of the optimization problem such that practical control systems are obtained.

Flight control designers have found it very difficult to overcome these problems when trying to exploit performance improvements and time savings offered by mathematical optimization. Modern control theory has developed rapidly over the last decade to the point at which optimal control synthesis is theoretically possible for a wide class of problems. A particularly well developed class are linear systems with constant or time-varying coefficients. The design objectives of the system to be optimized must be expressed in terms of a performance criterion (PC) of specific quadratic form. The control system is considered optimal if its control law minimizes the PC evaluated over total mission time. The optimal control law can be shown to be a linear feedback law of all the n state variables of an n^{th} order system. Three major flaws preclude direct application of this theory as an advanced design tool:

- n feedback channels are required to optimally control an n^{th} order system.
- The prescribed form of the PC makes it very difficult to express design objectives in the required mathematical form.
- The computational load is high. Complex digital programs are required which, in turn, require long computing time, hence any system modifications require time-consuming program changes.

It is easy to see that even for simple system representations, controllers too complex for flight control mechanization are produced.

The objectives of this study were to alleviate all of these difficulties. Specifically, the objectives were to:

- Develop a practical controller design procedure based on modern control theory and powerful gradient techniques with performance criteria specified directly in terms of design objectives.
- Apply this procedure to the design of a 3-axis attitude controller for the space shuttle ascent phase.
- Validate design criteria and design procedure by simulation and analysis.

These objectives were fully achieved.

PRACTICAL CONTROLLER DESIGN PROCEDURE

A new hybrid-computerized control system design tool developed under previous NASA contracts is used as the basic design procedure. The application study to shuttle ascent control was performed in two study phases. The design goal of the first study was to minimize the dominant structural loads during atmospheric flight. Study Phase 2 design criteria are aimed at maximizing payload injected into orbit as affected by the flight control system. Another objective during both study phases was that control system sensitivity to off-nominal environmental characteristics be minimized.

An abbreviated breakdown of the design procedure is given below:

1. Mathematical modeling of the vehicle perturbation equations of motion (2-DOF in Study Phase 1; 6-DOF in Study Phase 2) are defined with time-varying coefficients reflecting the vehicle and environmental changes during powered ascent.
2. Selection of a practical controller structure with a limited number of feedback channels which are easily implemented.

3. Formulation of design goals in terms of a positive definite performance criterion of otherwise free form. During Study Phase 1, peak structural loads at the booster-orbiter rear attachment points were chosen as the major performance criterion to be minimized. During Study Phase 2, all the dominant payload penalties as affected by the flight control system were selected as the major terms in the performance criterion to be minimized.
4. Repetitive hybrid simulation of vehicle dynamics during ascent in fast time scale (typically 1000 times real time).
5. Performance analysis at the end of each simulation based on the selected performance criterion (PC).
6. Functional minimization of the PC by: (a) systematic grid search in parameter space of the controller parameters to be optimally adjusted, and (b) gradient search to precisely locate the minimum.
7. Real time simulation and recording of the optimized systems on analog strip charts and on IBM 1108 digital programs to verify analog results.

An early MSFC inhouse fully reusable two-stage shuttle configuration was used during Study Phase 1, whereas Phase 2 was concerned with controller design for the MDAC-20 two-stage reusable shuttle configuration. By sequential operation of the optimization procedure over floating optimization intervals, time-varying controller gain schedules are obtained. Another option in the design technique allows for consideration of several flight conditions for controller design, thus reducing the sensitivity of the optimized system to uncertainties in vehicle parameters or environmental conditions.

SUMMARY OF RESULTS

It was found that realistic simulation of vehicle and control system dynamics combined with an iterative gradient minimization scheme while operating at 1000 times real time could produce the expected optimal time-varying control gain schedules with reduced sensitivity to assumed uncertainties in the environmental conditions. Study Phase 1, whereby the design

goal was to reduce bending loads at specified booster fuselage stations for two adverse wind conditions, revealed that near perfect tradeoffs in bending load reduction were possible for the two disturbances considered. For example, the bending loads due to a wind profile A were reduced from 74% to 39% of their admissible values and loads due to a wind profile B were reduced from 41% to the same peak of 39%. In every case, the optimization technique determined the best compromise in control gain selection which results in equal performance (i.e., bending loads in this case) for any of the assumed flight conditions. Also, the classical trend of load relief by lowering position feedback gains in the region of high dynamic pressure was observed in the shape of the time-varying gain schedules.

Study Phase 2, whereby the design goal was to maximize control system related payload injected into orbit, also proved to be successful. It was shown that meaningful performance criteria could be developed which are functions of payload sensitivities dependent on control system design. Such payload oriented formulation of performance criteria forces engineers of various disciplines (dynamics and control, structures, aerodynamics, trajectory optimization and guidance) to work in close cooperation during early stages of advanced vehicle design.

The main objective of this study was to extend this hybrid optimization technique to the status of being a dependable and economical design tool involving a total systems approach in early stages of complex vehicle design. This objective was realized by the results obtained during these two study phases.

OUTLINE OF THE REPORT

This report is divided into two volumes. Volume I presents a general discussion of the optimization technique in summary form and of the results obtained. Volume II presents a detailed description of the optimization technique, derivation of mathematical models, and outlines of the miscellaneous digital support programs.

● Volume I

Section 1 describes the optimization technique operating sequentially over a floating optimization time interval. Grid and gradient search operations, sensitivity reduction to uncertainties and performance evaluation capability are described briefly.

Section 2 deals primarily with mathematical models used. Included are the math models of the two-degree-of-freedom and six-degree-of-freedom shuttle ascent phase. The synthetic wind profiles used as environmental disturbances are presented. Structural loads at the booster/orbiter interface are analyzed and found to have a significant impact on structural booster weight and payload injected into orbit. The major payload sensitivities and their use in the PC to achieve this design goal are included.

Section 3 deals with results obtained from both study phases. Results from Phase I consisted of pitch controller design for maximum load relief based on an early MSFC shuttle configuration using the 2-DOF model. Results from Phase II were broader since the MDAC-20 shuttle configuration using the 6-DOF model was used. Pitch-controller design for maximum load relief was repeated to verify model and optimization technique. The remaining results are based on the second design goal of maximum payload injection into orbit. The pitch controller was optimized for headwinds and the yaw controller for sidewinds. The optimized systems were analyzed to verify desensitization to wind uncertainties.

Section 4 contains the conclusions and recommendations obtained from this study.

Section 5 contains all references.

● Volume II

Volume II, written in appendix form, was included as a detailed source of information on which this study was performed. Appendix A describes the hybrid optimization technique and its application to simple systems. All aspects of the technique are included. Appendix B details the derivation of the six-degree-of-freedom perturbation equations of motion describing the shuttle ascent. Appendix C presents the derivation of the equations of motion to determine structural interface loads at all four attachment points between the booster and orbiter. Appendix D shows the analog wiring diagrams for the six-degree-of-freedom equations of motion derived above, interface load computation and control system dynamics. Appendix E shows all raw mass, aerodynamic and trajectory data for the MDAC-20 configuration and the time-varying coefficients generated from this data in plot form. Appendix F shows results of a digital simulation of the shuttle ascent trajectory, attitude and interface loads in response to a 0-degree headwind and 90-degree sidewind for constant gain controllers, while Appendix G shows the same simulation results for optimal controller adjustments.

Section 1 HYBRID OPTIMIZER PROGRAM

1.1 BASIC SCHEME

The basic scheme of the Hybrid Optimizer program is a direct optimization method, whereby only forward integrations of the dynamic equations are performed. The vehicle system dynamics and control system loops are simulated on the analog console of a hybrid computer as shown schematically in Fig. 1-1. During each simulation, the performance is evaluated by computing the performance index, J , which has been selected to best reflect the design objectives. After the simulation, J is transferred to the digital console where a minimization scheme is programmed to determine the minimum of J with respect to the adjustable parameters, namely the controller gain slopes.

1.2 UPDATE INTERVAL

During development of the hybrid optimizer, it was found that optimality didn't suffer if the optimization was carried out independently over a number of limited time intervals rather than simultaneously over the entire flight time. For this study, the total flight time was therefore divided into a finite number of update intervals of length $(t_{\nu+1} - t_{\nu}) = \Delta t$ of typically 5 seconds as indicated in Fig. 1-2.

While rigorous optimal gain schedules as obtained from calculus of variations will be general functions of time, the class of optimal gain schedules to be generated by the present method was restricted to piecewise linear functions of time as in Fig. 1-2. This largely reduces the computational load and at the same time keeps the resulting optimal schedules closer to a practical form more suitable for implementation. Piecewise constant schedules,

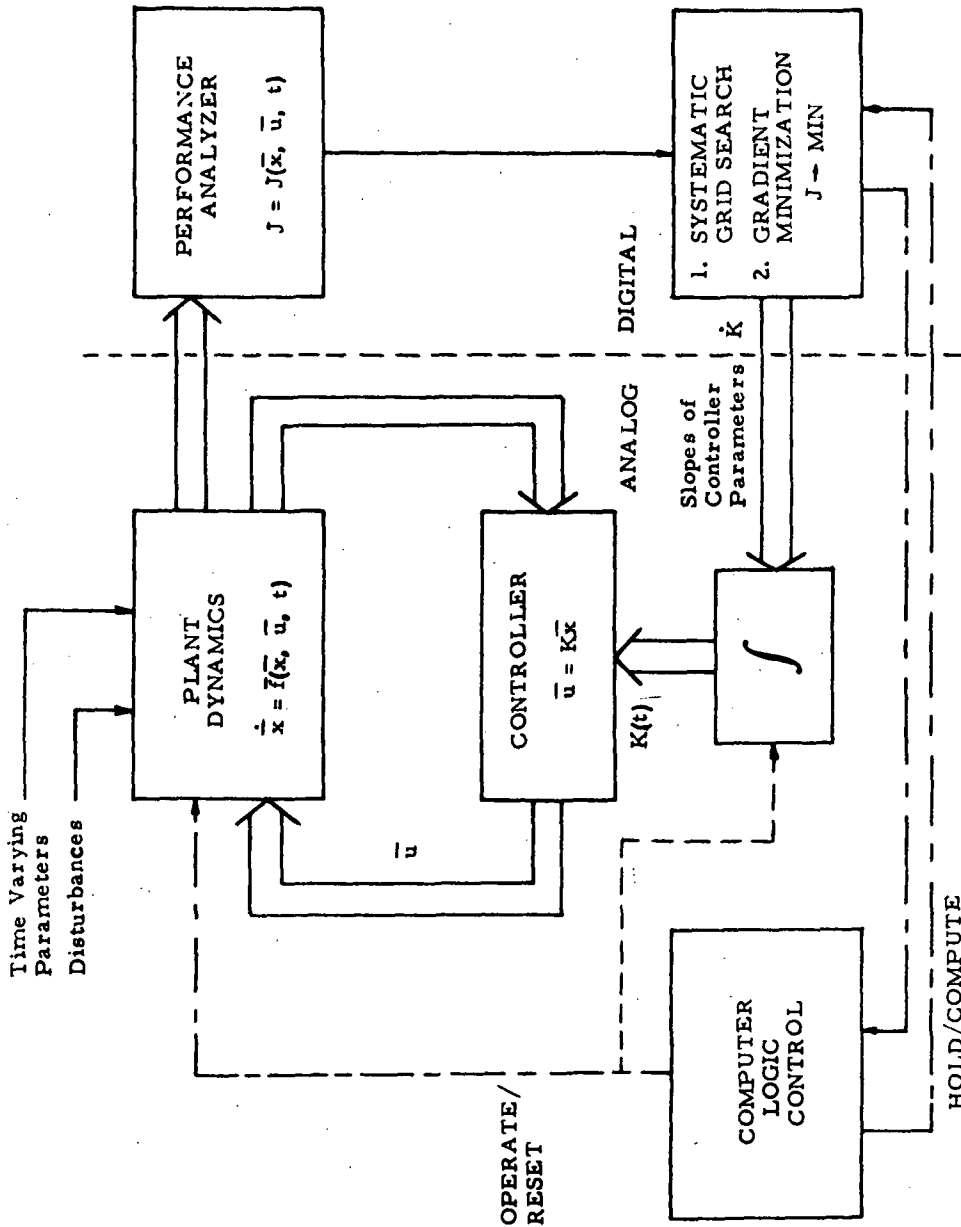


Fig. 1-1 - Basic Control System Optimization Scheme. Complete plant and control system dynamics are simulated repetitively on analog console of hybrid computer. Performance is analyzed after simulation in digital computer and optimized by iterative changes in slopes of controller gain schedules.

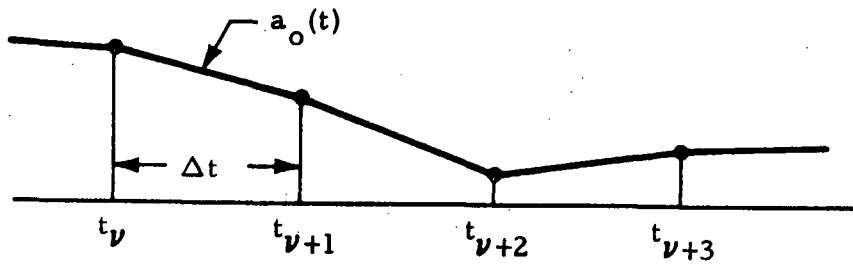


Fig. 1-2 - Desired Polygonal Form of Optimal Gain Schedules

as defined at break points $t_\nu, t_{\nu+1}, \dots$, have been found to be unacceptable in this approach because of the transients generated from large numbers of step-type gain changes.

1.3 OPTIMIZATION INTERVAL

At each update time, t_ν , the optimizer performs a series of fast-time forward integrations while iteratively adjusting the controller gain slopes in order to evaluate the vehicle performance. A minimum duration is required for these forward integration intervals. Methods to establish this minimum look-ahead time interval, T , were discussed in Section 6 of Ref. 5. For the shuttle dynamics, the minimum value of T which sufficiently detects the significant effects of a particular set of gain schedules is between 15 and 20 sec. Figure 1-3 shows a general example.

As sketched in Fig. 1-4, a number of slopes for each controller gain is simulated by fast-time forward integrations of the system dynamics with period T . The gradient optimization technique chooses the optimum slope originating at t_ν , based on the J function, then the system dynamics are integrated in real time to $t_{\nu+1}$ at which time the process is repeated. Final optimization results yield for each controller gain being optimized a polygonal form as shown in Fig. 1-2.

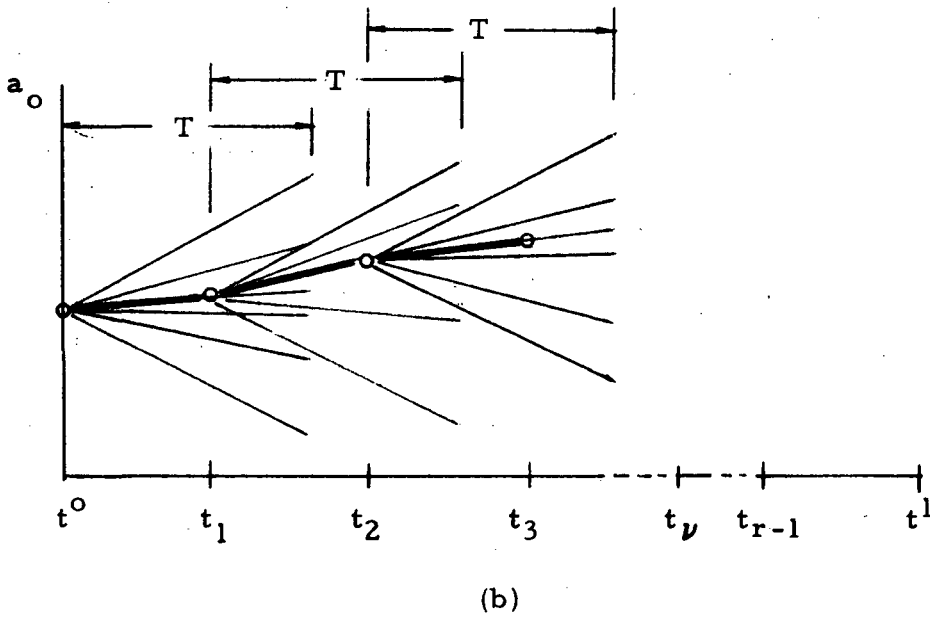
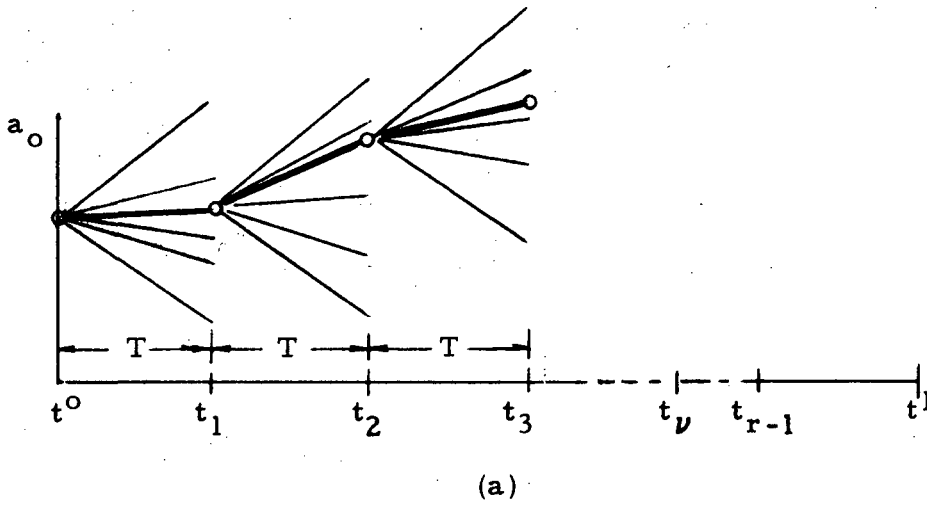


Fig. 1-3 - Total Mission Time (t^0, t^1) Broken Down into Finite Number r of Updating Intervals $(t^0, t_1), (t_1, t_2), \dots, (t_\nu, t_{\nu+1}), (t_{r-1}, t^1)$. Optimization Intervals $(t_\nu, t_\nu+T)$ are identical to updating intervals $(t_\nu, t_{\nu+1})$ as in Fig. 1-3(a) or are longer than updating intervals (Fig. 1-3(b)).

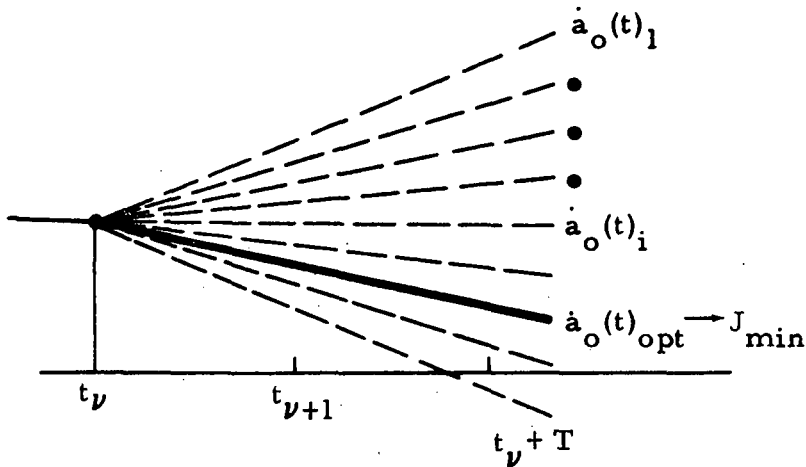


Fig. 1-4 - During Optimization Cycle at Flight Time, t_ν , a Large Number of Linear Gain Schedules are Evaluated for their Load Relief Performance

1.4 GRID SEARCH

In earlier development stages of the optimizer, it was found that the gradient technique ran the risk of finding local minima rather than absolute minima for given dynamics and performance index J . Modifications to avoid this problem resulted in a systematic grid search being added to the program. A two-dimensional case is shown in Fig. 1-5. This modification resulted into two basic optimization steps at each update interval t_ν :

- **Systematic Grid Search**

All possible parameter combinations within a grid of specified limits and fineness are evaluated for J . This complete survey of parameter space largely reduces the risk of finding local rather than absolute minima.

- **Gradient Search**

A powerful gradient minimization scheme based on the method of conjugate gradients (Ref. 2) uses the minimum of the grid search as starting point for a modern method of steepest descent to locate the minimum more precisely.

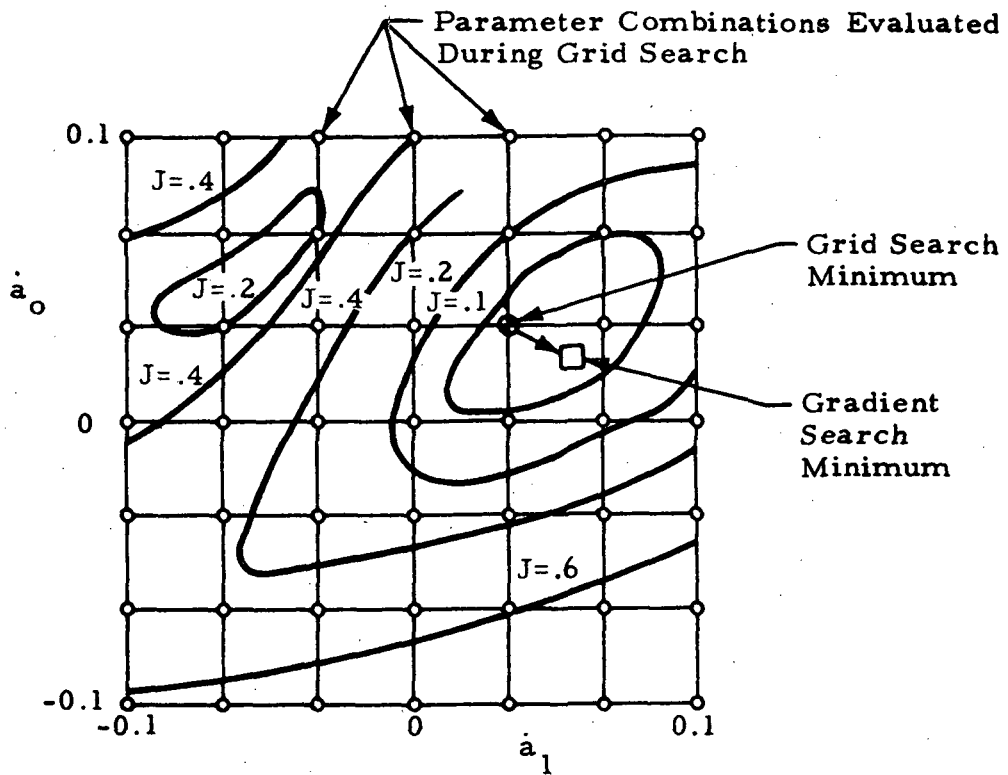


Fig. 1-5 - Parameter Optimization Performed in Two Phases: (1) Systematic Grid Search (o) for Complete Survey of Parameter Space; Grid Point of Minimum J (●) Serves as Starting Point for (2) Gradient Search Which Locates the Minimum More Precisely (□). From Grid Search Contour Plots (Lines of $J = \text{Const}$) can be Drawn for Better Insight into J -Topology.

1.5 REDUCING THE SENSITIVITY TO PARAMETER UNCERTAINTIES

The hybrid optimizer has the capability to design a truly optimal system; that is, one which anticipates the occurrence of a number of possible conditions, tests performance against a criterion which is a function of these possible conditions, and adjusts the control parameters so as to optimize this performance criterion. For example, in the case of launch vehicle control systems, it might be desirable to minimize peak bending moments assuming the possible occurrence of a variety of different environmental or failure conditions. This concept has been aptly described as "optimizing the compromise." Optimization results to be discussed in later sections will verify this concept.

This capability of "Parameter Uncertainty Desensitization" was easily added to the optimizer. Instead of considering only one operating condition, the optimizer was modified to consider two conditions which may be defined as the two most adverse operating conditions. At each grid point, both conditions are simulated, and the worst condition is chosen as the condition to be optimized. The gradient search performs in the same manner except when gradients are being computed. Experience had proven that no radical change in performance could be detected by the small perturbations of the controller gain slopes needed to compute gradients. This method of considering two adverse operating conditions can be readily expressed as solving a "minimax" problem; i.e., minimizing the maximum of several functions.

1.6 PERFORMANCE EVALUATION

The most practical feature of this hybrid optimizer is the ability to specify design goals in the most direct manner with virtually no mathematical constraints concerning its functional form. This high degree of flexibility in selecting performance criteria of arbitrary form was fully utilized by choosing a minimax criterion for initial shuttle ascent studies. This criterion was found to be the most selective and most direct mathematical

representation of the design goal; i.e., reduce shuttle peak bending loads at the worst of several stations along the vehicle, namely the interface connections of the orbiter to booster.

Section 2
MATHEMATICAL MODELS

Initial objectives were to extend, refine, and apply the optimization technique to the thrust vector attitude stabilization of a large two-stage space shuttle during atmospheric ascent with a distinct design goal of minimizing structural loads under a wide range of adverse wind conditions.

This section shows the initial simplified pitch plane model used to begin these studies. Expansion to full 6-D dynamics are included in the latter part of this section.

2.1 TWO-DEGREE-OF-FREEDOM MODEL

A set of simplified rigid-body perturbation equations were derived for use in this first study phase. The equations listed as follows describe the perturbation dynamics about a nominal pitch plane trajectory; i.e., lateral drift in position and pitch angle attitude.

Shuttle Dynamics

$$\ddot{z} = k_1 \phi + k_2 \alpha + k_3 \beta$$

$$\ddot{\phi} = -c_1 \alpha - c_2 \beta$$

$$\alpha = \phi + k_v \dot{z} + \alpha_w$$

Trim Equations

$$(T - X_a) \alpha_o + \bar{q} S C_{N_\alpha} \alpha_o + \frac{CT}{F} \beta_o = 0$$

$$(T - X_a) d - (\ell_r C_{N_\alpha} + \ell C_{m_\alpha}) \bar{q} S \alpha_o - \ell_\beta \frac{CT}{F} \beta_o = 0$$

Control Law

$$\beta_c = a_0 \phi + a_1 \dot{\phi} + g_2 \ddot{z}_a$$

$$\ddot{z}_a = \ddot{z} + k_{cg} \ddot{\phi} + k_1 \phi$$

$$\beta = H_\beta(s) \beta_c$$

where

$$k_1 = - \frac{T - X_a}{m}$$

$$k_2 = \frac{-\bar{q} S C_{N\alpha}}{m}$$

$$k_3 = - \frac{CT}{Fm}$$

$$c_1 = \frac{+\bar{q} S C_{N\alpha} (X_{cg} - X_{cp})}{I}$$

$$c_2 = (x_{cg} - x_E) \frac{CT}{FI}$$

$$k_v = \frac{1}{U_o}$$

$$k_{cg} = x_{cg} - x_a$$

$$H_\beta(s) = \frac{15}{S+15}$$

and

T = total thrust of engines

X_a = total aerodynamic drag

\bar{q} = dynamic pressure

S = reference planform area

C_m = pitching moment coefficient

C_{m α} = $\partial C_m / \partial \alpha$

C_N = normal force coefficient

C_{N α} = $\partial C_N / \partial \alpha$

H _{β} (s) = actuator dynamics

X_{cg} = longitudinal location of center of gravity from gimbal

X_{cp} = longitudinal location of center of pressure from gimbal

x_E = gimbal location

U_o = nominal velocity

x_a = accelerometer location

α_o = trim angle of attack

C = number of gimbaled engines

F = total number of engines

β_o = trim gimbal angle

d = offset of gimbaled engines from vehicle axis

l = reference length (body length)

l_R = distance from cg to moment reference point

l _{β} = distance from cg to gimbal point of engine

Sign conventions and notations are shown in Fig. 2-1. The equations of motion describing the trim attitude of the vehicle were derived and simulated as required to properly describe the desired bending moments. The bending moment equations were formulated in a simplified form as follows:

$$\frac{M_{B_i}}{M'_{\beta_i}} = \frac{M'_{\alpha_i}}{M'_{\beta_i}} (\alpha + \alpha_o) + \beta + \beta_o$$

$$i = 1, N \quad \text{where } N = \text{number of critical stations}$$

A simplified block diagram shown in Fig. 2-2 shows the method of analog simulation.

2.2 SIX-DEGREE-OF-FREEDOM MODEL

A set of 6-DOF rigid body perturbation equations were derived for use in the second phase of this study. A detailed derivation of these equations is provided in Volume II of this report. These equations describe the 6-DOF perturbation dynamics about a nominal ascent trajectory and are listed as follows:

Shuttle 6-DOF Dynamics

$$\ddot{x} = -k_{\phi} \dot{\theta} - k_3 \alpha + k_{xc} \delta_c + k_{xe} \delta_e$$

$$\ddot{y} = k_{\phi} \dot{\phi} + k_{\psi} \dot{\psi} + k_1 \delta_{\psi} + k_{y\beta} \beta + k_{ya} \delta_a + k_{yr} \delta_r + k_2 \psi + k_3 \phi$$

$$\ddot{z} = k_{\theta} \dot{\theta} - k_1 \delta_{\theta} + k_{z\alpha} \alpha + k_{ze} \delta_e + k_{zc} \delta_c$$

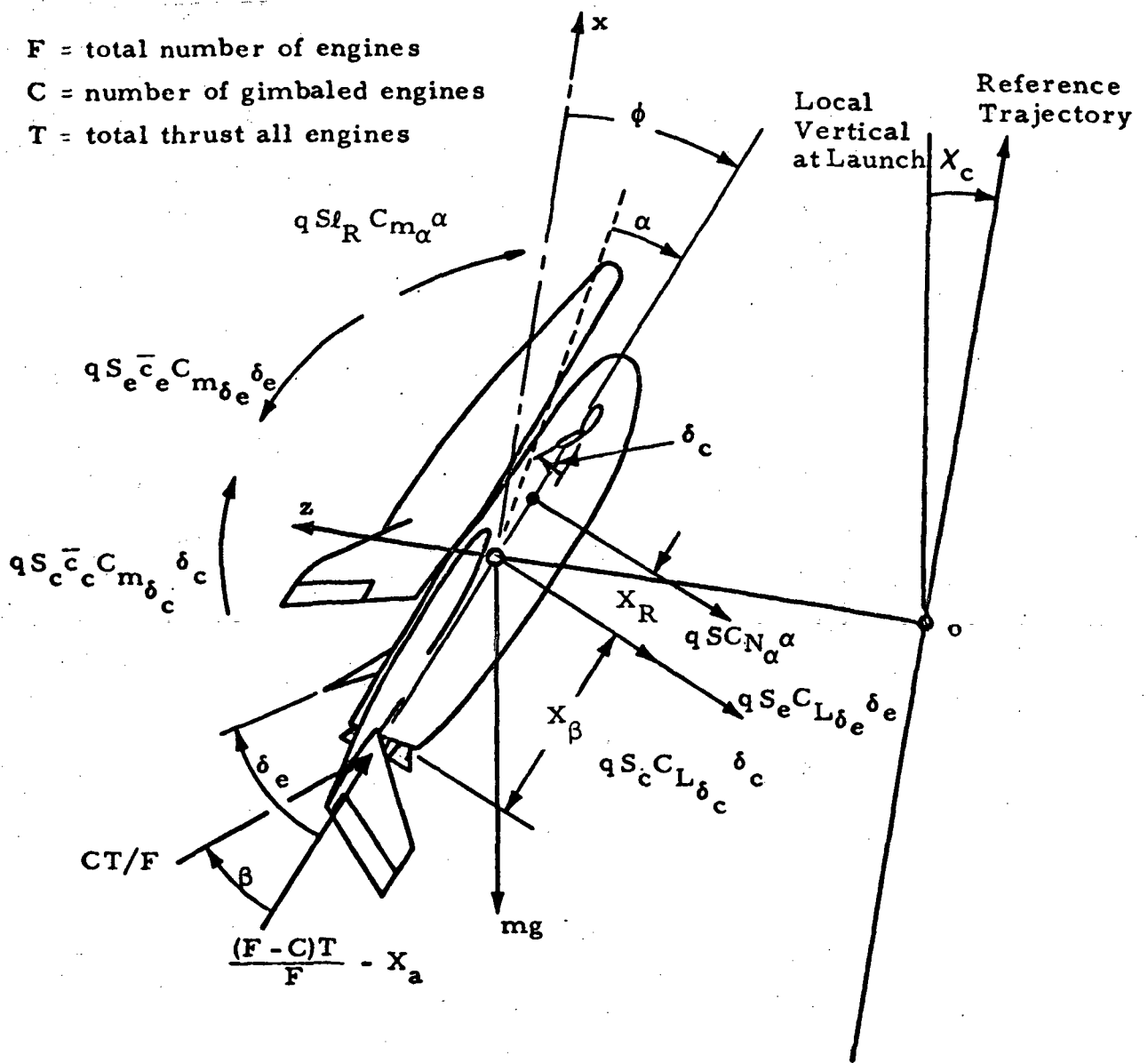


Fig. 2-1 - MSFC Space Shuttle Configuration Body Axis Representation Showing Sign Convention of Dynamic Equations

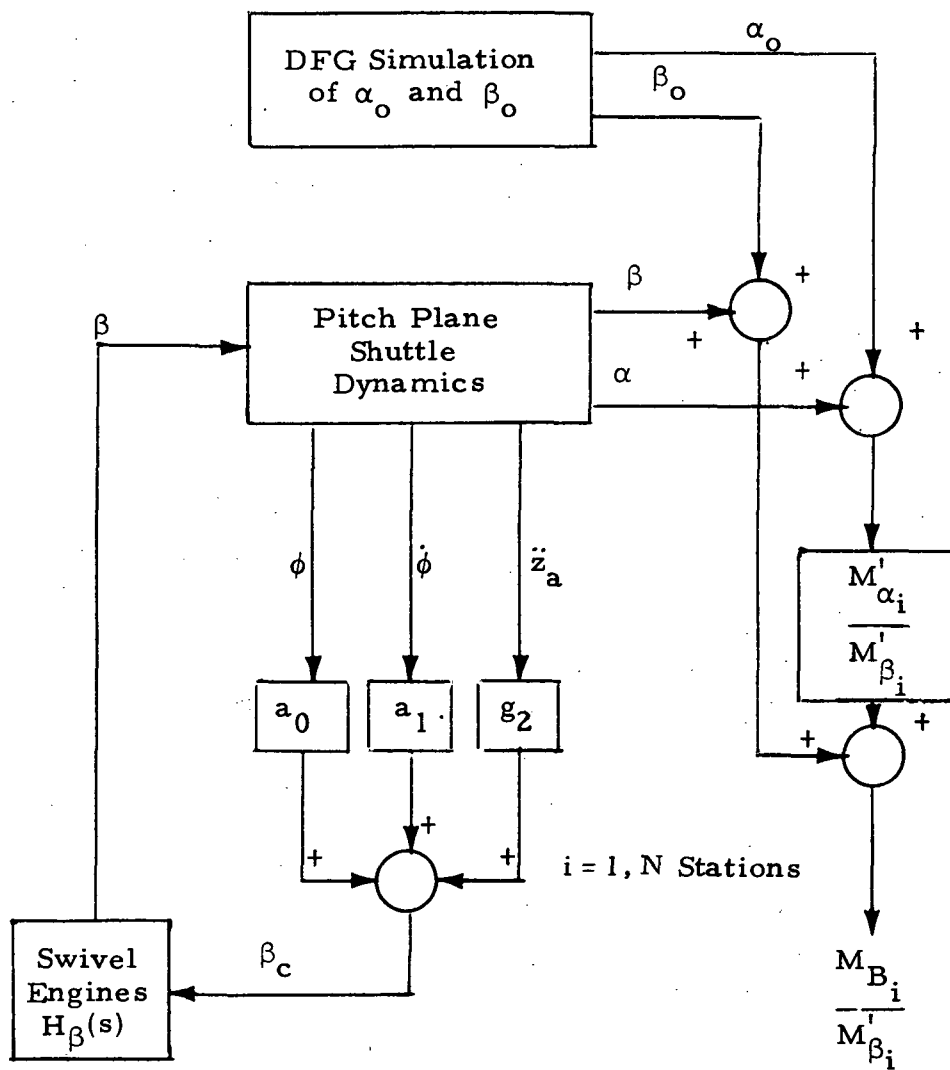


Fig. 2-2 - Block Diagram of Controller and Open-Loop Bending Computation for MSFC Shuttle Configuration

$$\ddot{\phi} = k_{\phi\psi} \ddot{\psi} + k_{l\theta} \delta_{\theta} + k_{l\psi} \delta_{\psi} + k_{l\phi} \delta_{\phi} + k_{l\dot{\phi}} \dot{\phi} + k_{l\dot{\psi}} \dot{\psi} + k_{l\beta} \beta + k_{la} \delta_a + k_{lr} \delta_r$$

$$\theta = k_{m\alpha} \alpha + k_{m\theta} \delta_{\theta} + k_{m\dot{\theta}} \dot{\theta} + k_{me} \delta_e + k_{mc} \delta_c$$

$$\ddot{\psi} = k_{n\psi} \ddot{\psi} + k_{n\dot{\phi}} \dot{\phi} + k_{n\dot{\psi}} \dot{\psi} + k_{n\beta} \beta + k_{na} \delta_a + k_{nr} \delta_r$$

$$\alpha = \theta - \alpha_w + u_{io} \dot{z}$$

$$\beta = -\psi - \beta_w + u_{io} \dot{y}$$

Control Law

$$\delta_{\theta} = -H_{\theta}(s) \left[a_{o\theta} \theta + a_{l\theta} \dot{\theta} \right]$$

$$\delta_{\psi} = -H_{\psi}(s) \left[a_{o\psi} \psi + a_{l\psi} \dot{\psi} - b_{o\psi} \beta \right]$$

$$\delta_{\phi} = -H_{\phi}(s) \left[a_{o\phi} \phi + a_{l\phi} \dot{\phi} \right]$$

$$\delta_c = -k_c H_c(s) \left[a_{o\theta} \theta + a_{l\theta} \dot{\theta} \right]$$

$$\delta_e = -k_e H_e(s) \left[a_{o\theta} \theta + a_{l\theta} \dot{\theta} \right]$$

$$\delta_r = -k_r H_r(s) \left[a_{o\psi} \psi + a_{l\psi} \dot{\psi} - b_{o\psi} \beta \right]$$

$$\delta_a = -k_a H_a(s) \left[a_{o\phi} \phi + a_{l\phi} \dot{\phi} \right]$$

Trim Equations

$$k_{z\alpha} \alpha_o - k_{l1} \delta_{\theta_o} + k_3 + k_{n_o} - U_o \dot{\chi}_{\theta} = 0$$

$$k_{m\alpha} \alpha_o + k_{m\theta} \delta_{\theta_o} + k_{m_o} - \frac{T \cdot \Delta Z_{cg}}{I_y} = 0$$

The bending load EOM of the fuselage due to pitch plane dynamics were identical to the simplified pitch plane study with the exception of terminology describing engine deflection.

$$\frac{M_{B_i}}{M'_{\beta_i}} = \frac{M'_{\alpha_i}}{M'_{\beta_i}} (\alpha + \alpha_o) + (\delta_{\theta} + \delta_{\theta_o})$$

The trim conditions were computed in the same manner as previously. Figure 2-3 shows the sign conventions and notations used.

2.3 SYNTHETIC WIND PROFILES

Four wind profiles referenced to various time points of the MSFC shuttle reference trajectory (3g limit) were derived and are shown in Fig. 2-4. A reverse shear (wind build-up rate) profile was also constructed and is shown in Fig. 2-5.

A derivation was performed to convert these winds from (wind velocity versus altitude) to (angle of attack relative to vehicle versus flight time). This derivation is included in Volume II. The resulting equation is:

$$\alpha_w \approx \tan^{-1} \left(\frac{V_w \cos \chi_\theta}{V + V_w \sin \chi_\theta} \right) + \frac{\dot{z}}{V}$$

where

χ_θ is command pitch angle from local vertical

V_w is wind velocity

V is nominal forward velocity vector

\dot{z} is lateral drift

Two winds were chosen as the adverse conditions to be used in the optimization studies. They are identified in Fig. 2-6.

2.4 BOOSTER/ORBITER STRUCTURAL INTERFACING LOADS

Since the ultimate design goal of maximization of orbit insertion weight was the primary objective of optimal attitude control during powered ascent, it was necessary to develop a performance index function which realizes this goal. Engineering experience had shown that the major insertion weight

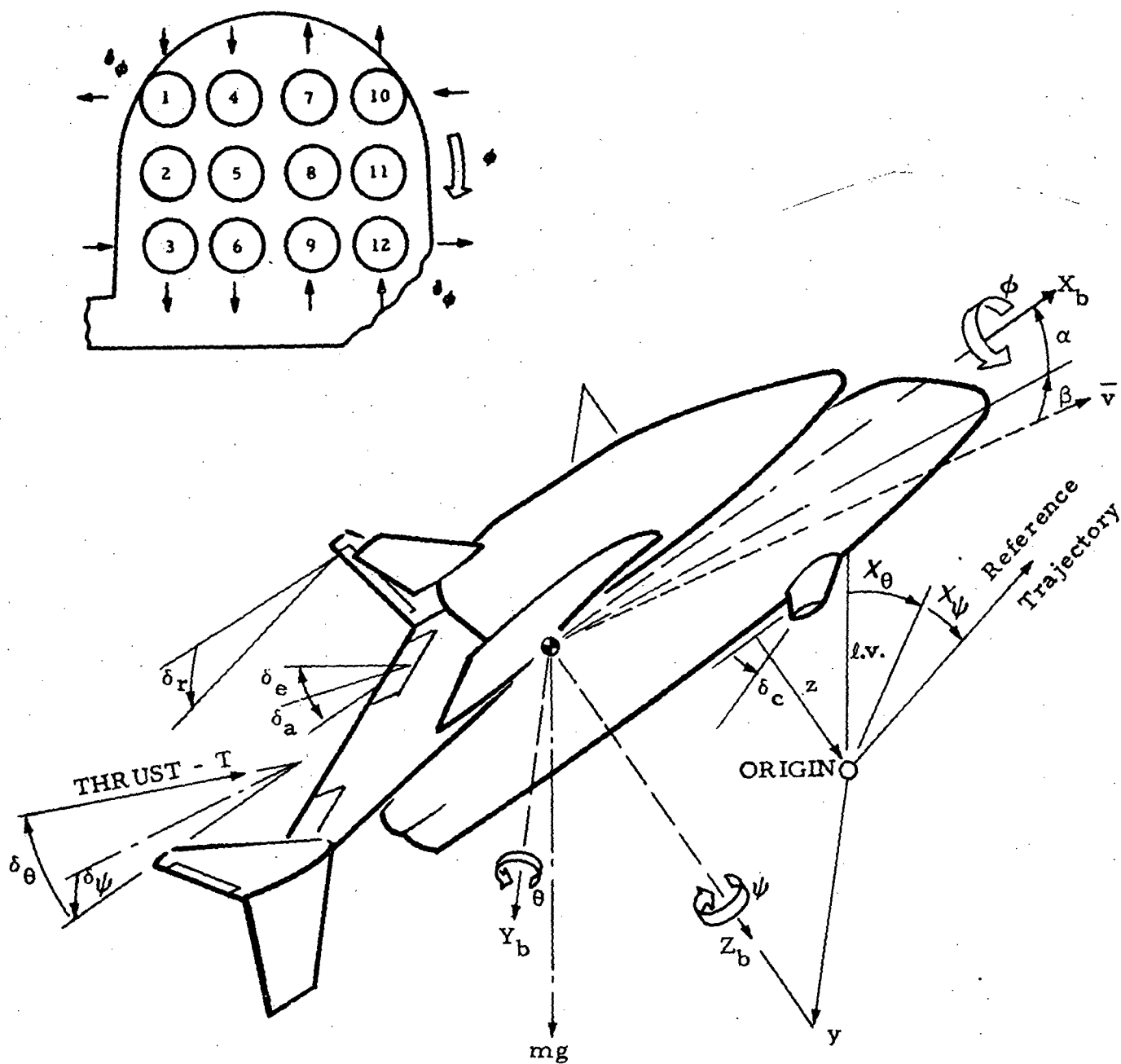


Fig. 2-3 - Sign Conventions and Notations for 6-Degree-of-Freedom Shuttle Ascent Perturbation Equations of Motion

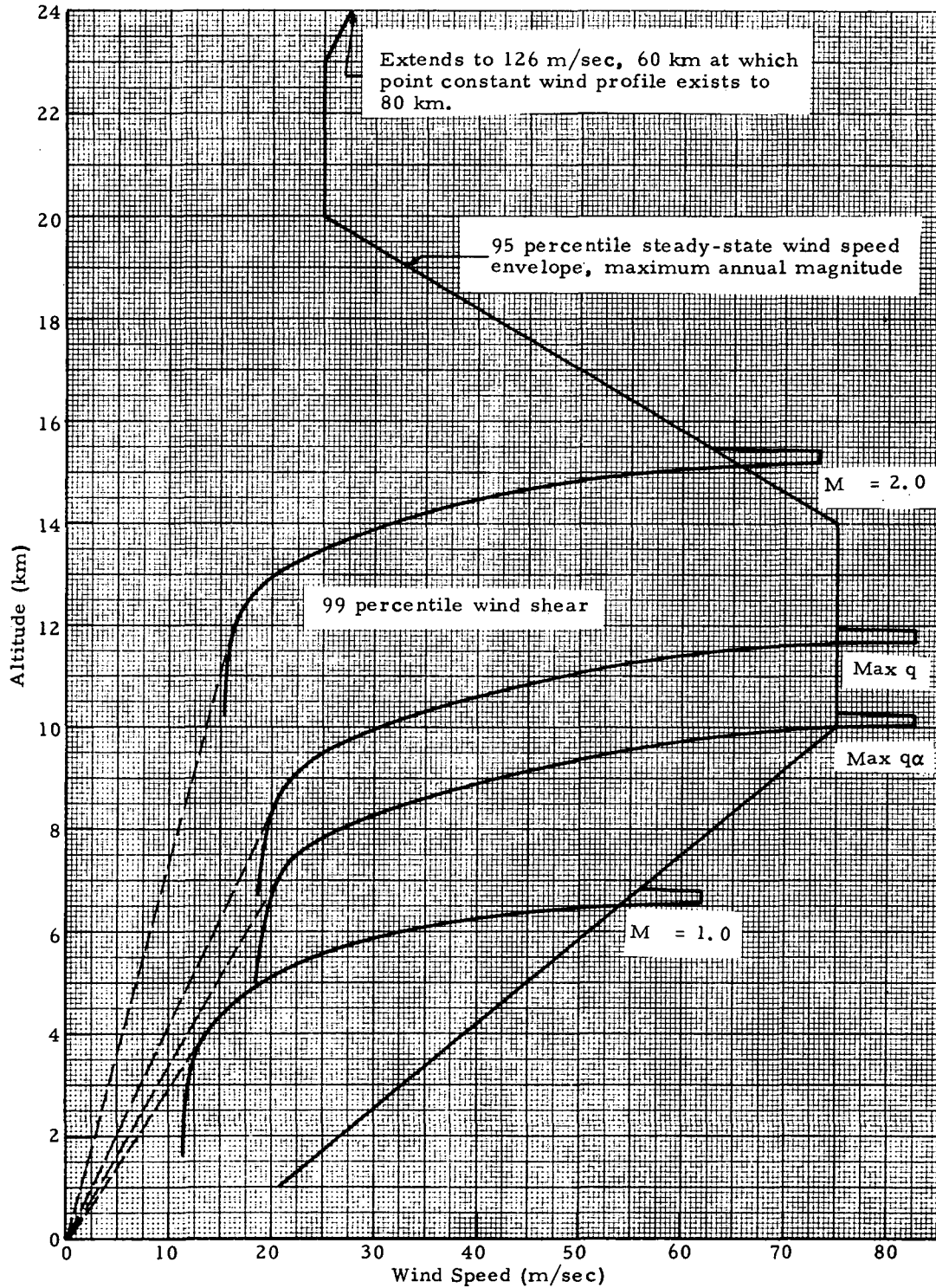


Fig. 2-4 - MSFC 95% Synthetic Wind Profiles - Maximum Annual Magnitudes. Profiles Generated Using Data and Directions Contained in Ref. 6. (M = Mach number)

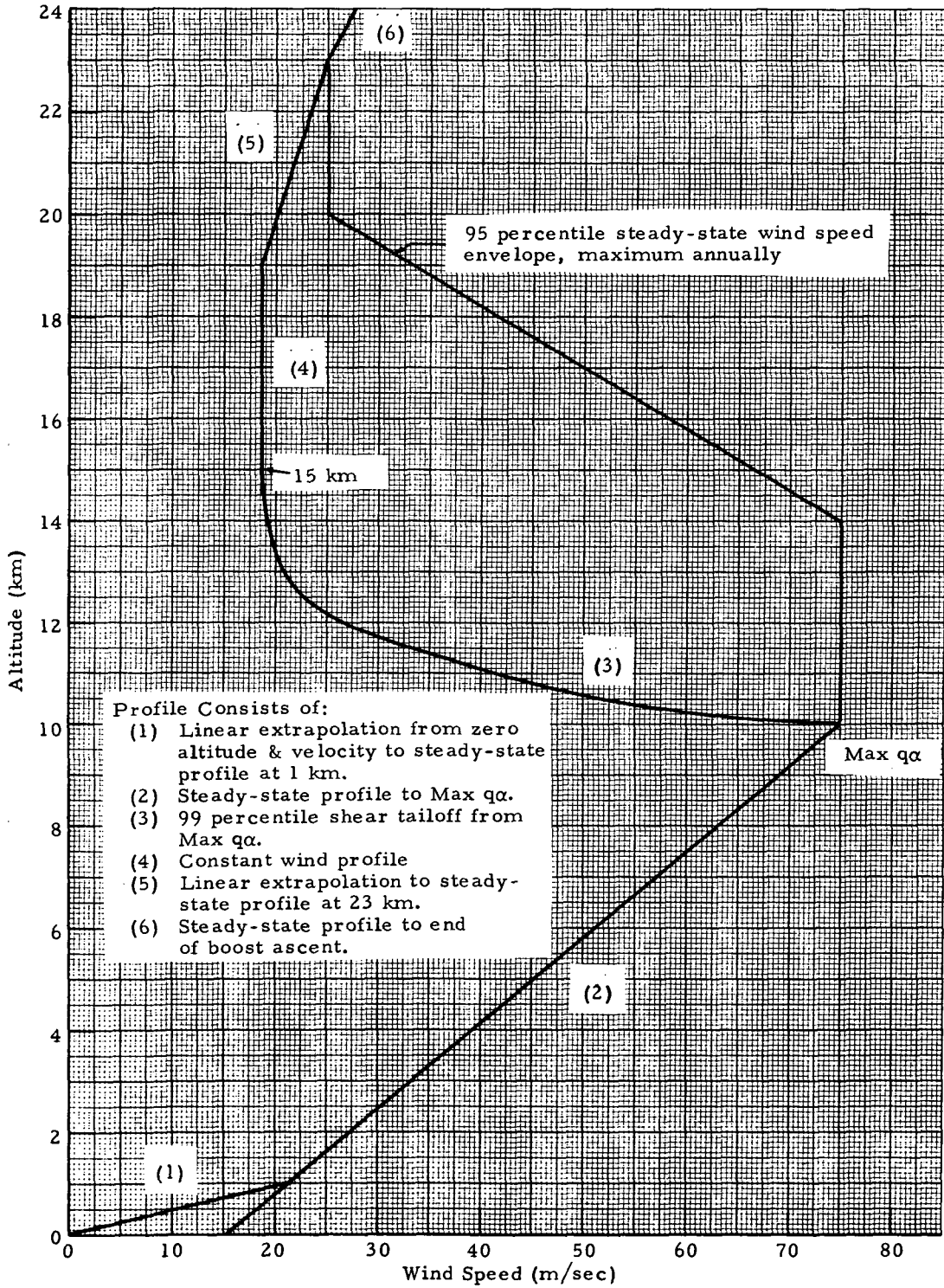


Fig. 2-5 - Reverse Shear Synthetic Wind Profile

SHUTTLE BOOST ASCENT

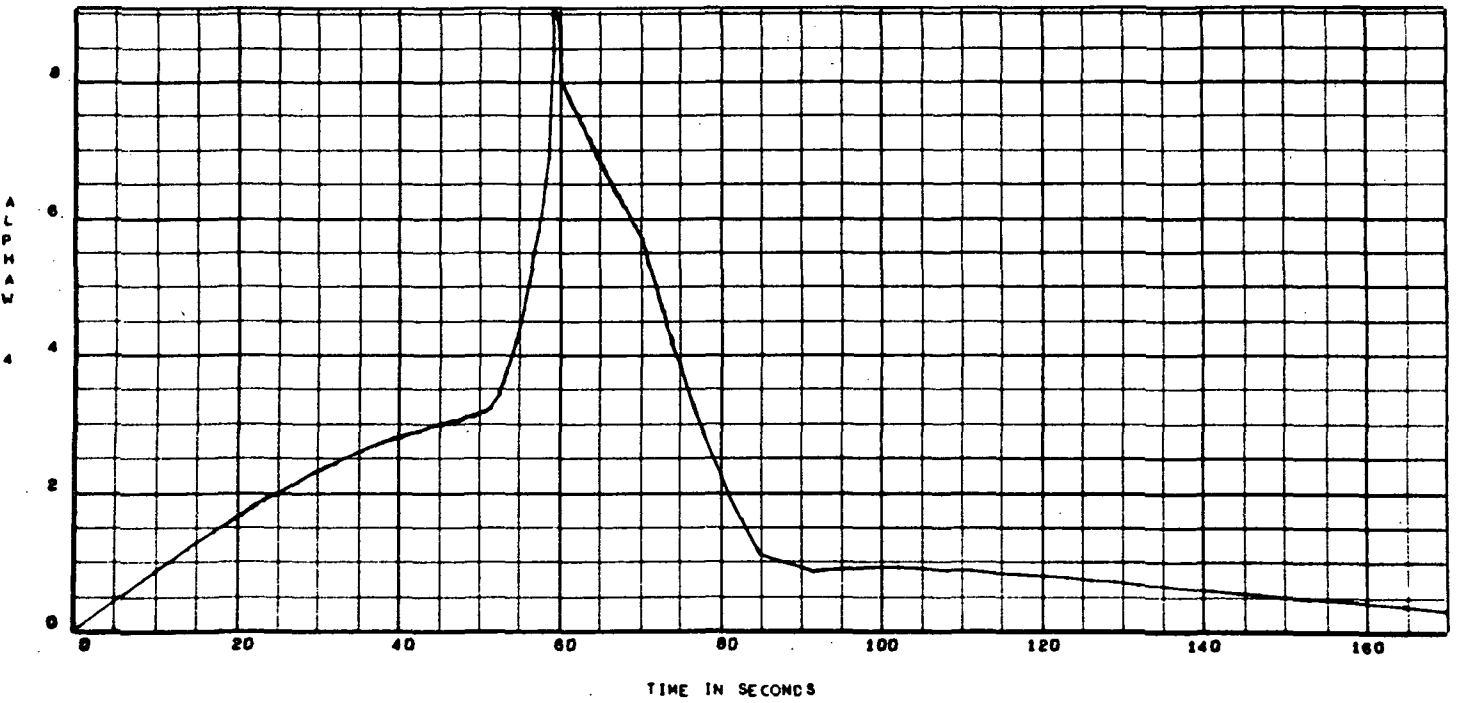
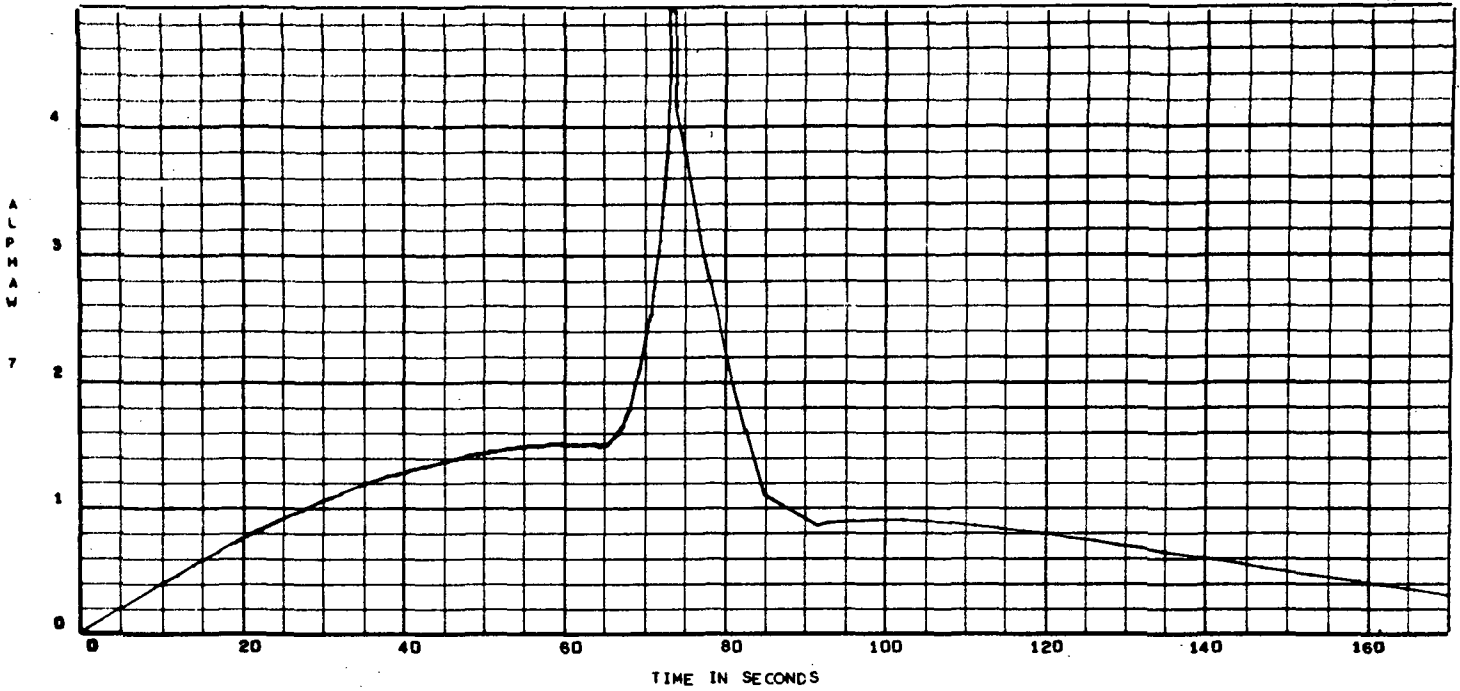


Fig. 2-6 - Adverse Wind Profiles Used in Entire Present Study: α_{w4} selected as Wind Disturbance A and α_{w7} selected as Wind Disturbance B

α_{wA} = 95 percentile maximum annual steady-state wind with 99 percentile maximum shear and superimposed gust at maximum \bar{q} ; α_{wB} = 95 percentile maximum annual steady-state wind with 99 percentile maximum shear with superimposed gust at Mach 2.

penalty contribution would be the booster dry weight which is dependent upon the structural loads encountered during powered ascent. The interface loads transmitted through the attachment points between booster and orbiter were identified as having a strong impact on the booster fuselage weight. It was therefore necessary for the equations of motion describing these interface loads to be derived and extended to the hybrid simulation studies to allow for continuous computation of these loads for vehicle performance evaluation. The general approach to the development of these interface equations are given in the following paragraphs. A more detailed derivation is included in Volume II of this report.

The structural design of the supports between booster and orbiter depend on the maximum interface loading on each of the supports during the entire ascent phase of the flight. Knowing the motion of the composite vehicle (\vec{U}, \vec{Q}) from the 6-D ascent simulation for the nominal trajectory, the nominal interface forces and moments can be determined as part of the external forces acting on the orbiter only (subscript o) which lead to the orbiter's known motion \vec{U}_o, \vec{Q}_o :

$$(\vec{F})_I = (M)_o \left[\dot{\vec{U}} + \vec{Q} \times \vec{U} \right] - (\vec{F}_{aero})_o - (\vec{F}_{cg \text{ offset}})_o - (\vec{W})_o$$

$$(\vec{M})_I = [I_o] \dot{\vec{Q}} + \vec{Q} \times [I_o] \vec{Q} - (\vec{M}_{aero})_o$$

For the actual trajectory (i.e., perturbed trajectory), the perturbed interface forces and moments are given by

$$(\vec{f})_I = (M)_o \left[\dot{\vec{u}} + \vec{Q} \times \vec{u} + \vec{\omega} \times \vec{U} \right] - (f_{aero})_o - (f_{cg \text{ offset}})_o - (\vec{w})_o$$

$$(\vec{m})_I = [I_o] \dot{\vec{\omega}} + \vec{\omega} \times [I_o] \vec{Q} + \vec{Q} \times [I_o] \vec{\omega} - (\vec{m}_{aero})_o$$

where capital letters and lower case letters indicate nominal and perturbed values, respectively, and \vec{F}_I and \vec{M}_I are interface forces and moments.

$(F_{aero})_o$ and $(M_{aero})_o$ are the aerodynamic forces and moments acting on the orbiter alone. $(\vec{F}_{cg\ offset})_o$ is the centrifugal force due to offset of orbiter cg from that of the composite vehicle, and $(\vec{W})_o$ is the weight of the orbiter. The nominal interface forces and moments will be determined by the 6-D Shuttle Data program, whereas the perturbed forces and moments can be obtained from the analog simulation. The force components acting on each support, as shown in Fig. 2-7, can be determined by

$$\vec{R} = [A] (\vec{FM})_I + [A] (\vec{fm})_I$$

where

$\vec{R} = (R_{1x}, R_{1y}, R_{1z}, R_{2z}, R_{3z}, R_{4y})$ are force components acting on the supports

$[A]$ is a 6×6 matrix, where elements are functions of l_1, l_2, l_3, l_4

$\vec{FM} = ((\vec{F})_I, (\vec{M})_I)$

$\vec{fm} = ((\vec{f})_I, (\vec{m})_I)$

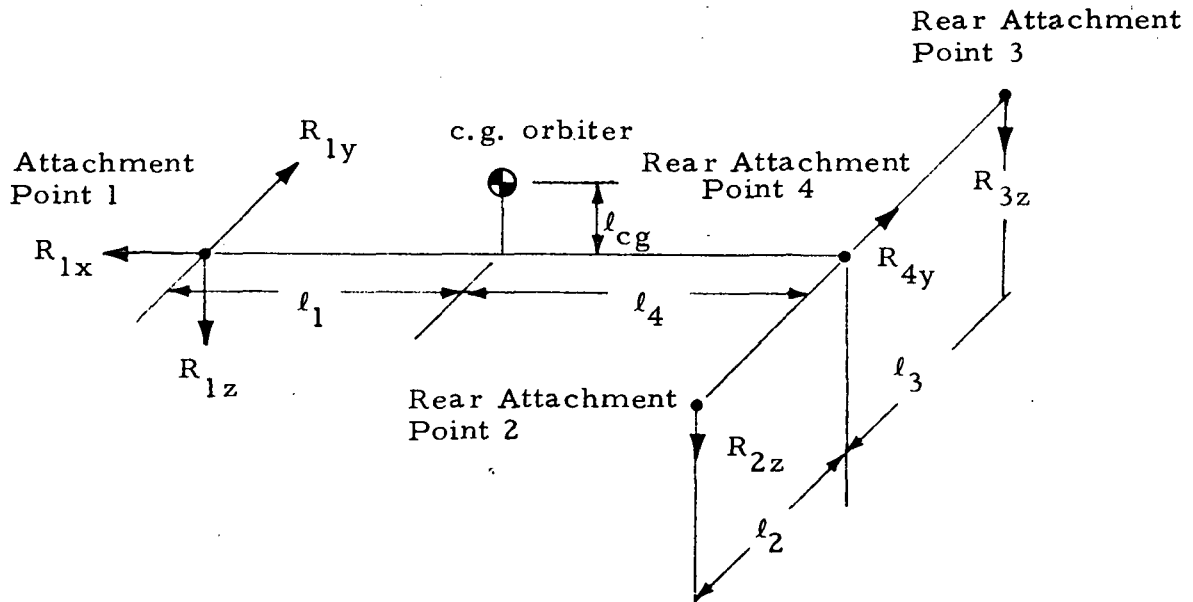


Fig. 2-7 - Components of Interface Load at the Attachment Points of Shuttle Booster and Orbiter (MDAC-20 Configuration)

This derivation yields the total interface force at each station as listed as follows.

$$R_{1x} = f_{x1} + F_{x1}$$

$$R_{1z} = g_1(f_{z1} + F_{z1}) + g_2 R_{1x} + g_3(\hat{m}_1 + M_1)$$

$$R_{1y} = g_4(\hat{n}_1) + g_5(f_{y1})$$

$$R_{4y} = f_{y1} - R_{1y}$$

$$R_{2z} = g_6 \hat{l}_1 + g_7 f_{y1} + g_8(f_{z1} + F_{z1}) + g_9 R_{1z}$$

$$R_{3z} = f_{z1} + F_{z1} - R_{1z} - R_{2z}$$

where

- | | |
|------------------------------|---|
| $g_1 = l_4 / (l_1 + l_4)$ | (lower case $f_{x1}, f_{y1}, \dots, \hat{m}_1$ indicate |
| $g_2 = l_{cg} / (l_1 + l_4)$ | perturbation interface forces and moments |
| $g_3 = -1 / (l_1 + l_4)$ | acting on body 1 (orbiter)) |
| $g_4 = 1 / (l_1 + l_4)$ | |
| $g_5 = l_4 / (l_1 + l_4)$ | |
| $g_6 = -1 / 2l_2$ | |
| $g_7 = -l_{cg} / 2l_2$ | |
| $g_8 = 1/2$ | |
| $g_9 = -1/2$ | |
| $F_{x1} =$ | nominal interface force along x-axis on body 1 (orbiter) |
| | due to trajectory and vehicle configuration |
| $F_{z1} =$ | nominal interface force along z-axis on body 1 (orbiter) |
| | due to trajectory and vehicle configuration |
| $M_1 =$ | nominal interface moment along y-axis on body 1 (orbiter) |
| | due to trajectory and vehicle configuration |

2.5 MAJOR PAYLOAD SENSITIVITIES

This section deals with methods of obtaining the orbit insertion weight partials for implementation into the performance index function to realize maximum orbital payload.

2.5.1 Impact of Structural Weight on Payload

A structural analysis of the booster fuselage in the region of the orbiter attachment points revealed that the peak interface forces R_{2z} , R_{3z} , R_{4y} strongly affect the booster hydrogen tank design shown in Fig. 2-8. The hydrogen tank is compression-critical rather than pressure-critical. The stress resultant N_x in the axial direction determines the design. In a first approximation, no circumferential variation was considered and N_x was determined by summing the effects of axial compression and bending from a one-dimensional internal load analysis. Given the maximum compressive loads, the stiffeners of each barrel can be designed by using the formulation given in Ref. 10. Three failure modes are considered: general instability, skin buckling, and web crippling. Their simultaneous occurrence determines the design point; i.e., the dimensions w , b , and t_s on Fig. 2-8. Then a weight thickness \bar{t} can be computed.

To find the variation of the tank weight with aft interface loads, the following procedure is followed:

1. For each flight condition of interest, the interface loads and the complete set of maximum axial compressive stress resultants N_x is computed.
2. The weight thickness of each barrel is determined.
3. The total tank weight is computed.

For the first step the internal shears and moments resulting from the external forces and moments must be determined. The external forces considered are distributed aerodynamic effects obtained from model measurements, inertia effects computed from the simulated accelerations and given mass

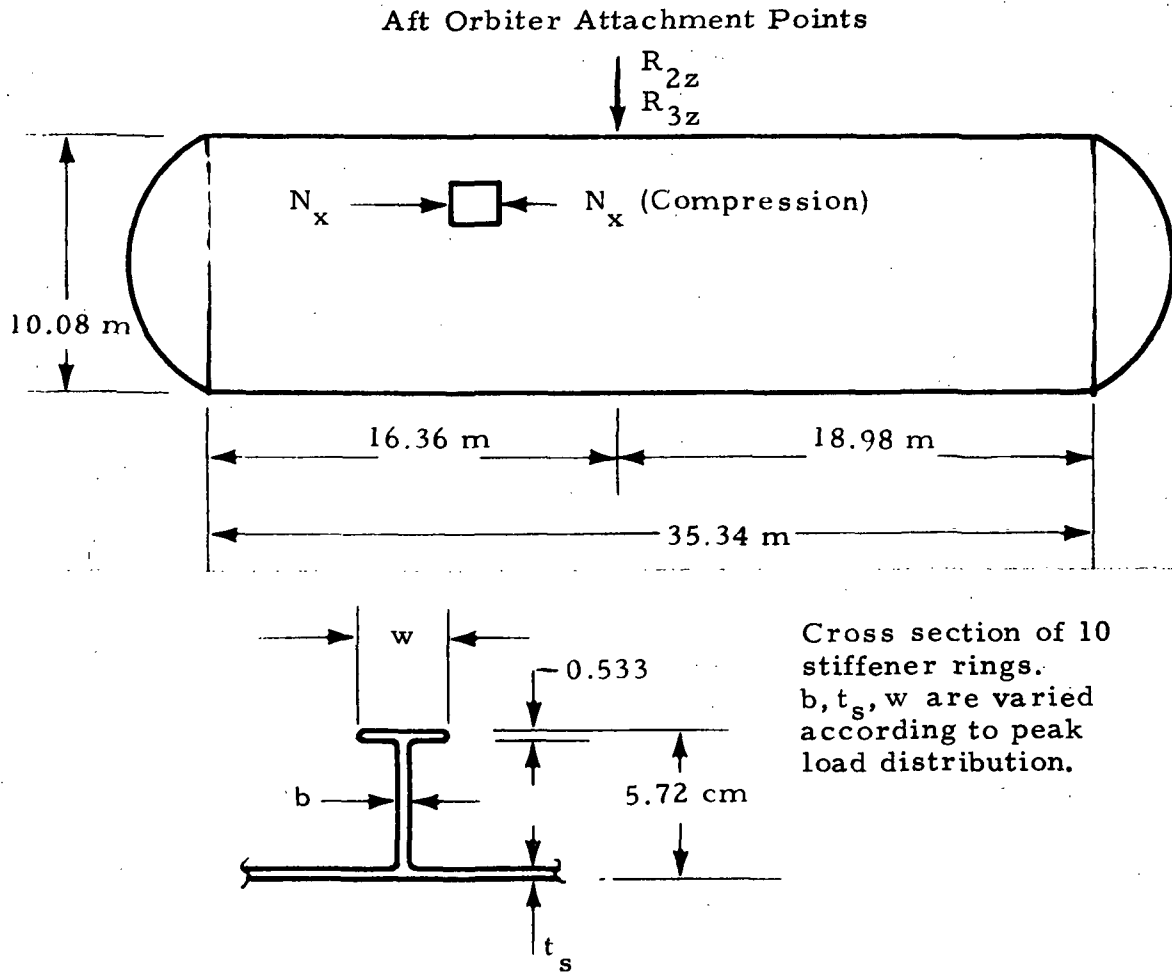
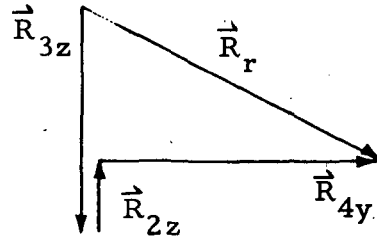


Fig. 2-8 - Booster Hydrogen Tank Stiffener Geometry

distribution. In order to account for general unsymmetrical loads, the total force at the three rear attachment points 2, 3, and 4 must be computed.

$$R_r = \sqrt{(R_{2z} + R_{3z})^2 + R_{4y}^2}$$



Peak values of R_r can then be used to determine the booster's H_2 -tank weight. The mass sensitivity of the booster H_2 -tank for changes in interface load R_r is then found to be

$$\frac{\Delta W_{H_2 \text{ Tank}}}{\Delta R_r} = 0.0104 \text{ Kg/N},$$

which can be expressed in a payload penalty ΔP according to Ref. 4.

$$\begin{aligned} \frac{\partial P}{\partial R_r} &\approx \frac{\Delta P}{\Delta R_r} = \frac{\Delta W_{H_2 \text{ Tank}}}{\Delta R_r} \frac{\Delta P}{\Delta W_{\text{Booster}}} = 0.0104 * 0.2 \\ &= 0.00208 \frac{\text{Kg}}{\text{N}} \end{aligned}$$

Since the tank center of gravity is only 0.6 m from the booster center of gravity upon burnout, no additional penalty due to hypersonic trim requirements is necessary.

2.5.2 Impact of Engine Gimbal Angle Requirements on Payload

The major effects of maximum engine gimbal angles on space shuttle payload were determined in a recent study (Ref. 12). An increase in engine deflection δ requires a heavier actuator system, larger engine base area with associated increase in drag, structural weight and fuel requirement.

Typical values for the payload penalty $\partial P/\partial \delta$ were found in Ref. 12 to be of the order

$$\frac{\partial P}{\partial \delta} = 221 \frac{\text{Kg}}{\text{deg}}$$

This value was also used in the present study for all total gimballed angles $\delta_{\text{Trim}} + \delta$ which exceed the nominal design values. Trim gimballed angles for the zero-lift trajectory used in the study (provided by MSFC, Aero-Astrodynamic Laboratory, Flight Mechanics Branch) are shown in Fig. 2-9.

2.5.3 Impact of Trajectory Deviations on Payload

Vehicle insertion weight variations from nominal, produced by vehicle state perturbations existing at the start of active closed-loop guidance, were assumed to be at $t_g = 100$ sec into ascent when atmospheric disturbances have virtually died out. These trajectory related penalty functions were computed using a trajectory computation program incorporating a quasi-optimal guidance concept. Insertion weight deviations were computed for each parameter of the vehicle state taken singly. The insertion weight was initially expressed by a quadratic function of the form

$$\Delta W_{\text{ins}} = \sum_{m=1}^3 \left[\frac{\partial W}{\partial x_m} x_m(t_g) + \frac{\partial W}{\partial v_m} v_m(t_g) + \frac{\partial W}{\partial x_m^2} x_m^2(t_g) + \frac{\partial W}{\partial v_m^2} v_m^2(t_g) \right]$$

Coupling terms had earlier been found to be insignificant for this particular reference zero lift trajectory provided by MSFC's Flight Mechanics Branch and were therefore neglected together with the quadratic terms which were two or more orders of magnitude smaller than the linear terms. The following payload penalty coefficients were calculated in second stage burn time and converted to payload penalty based on Ref. 11 for use in the performance criterion.

60 SHUTTLE BOOSTER ASCENT

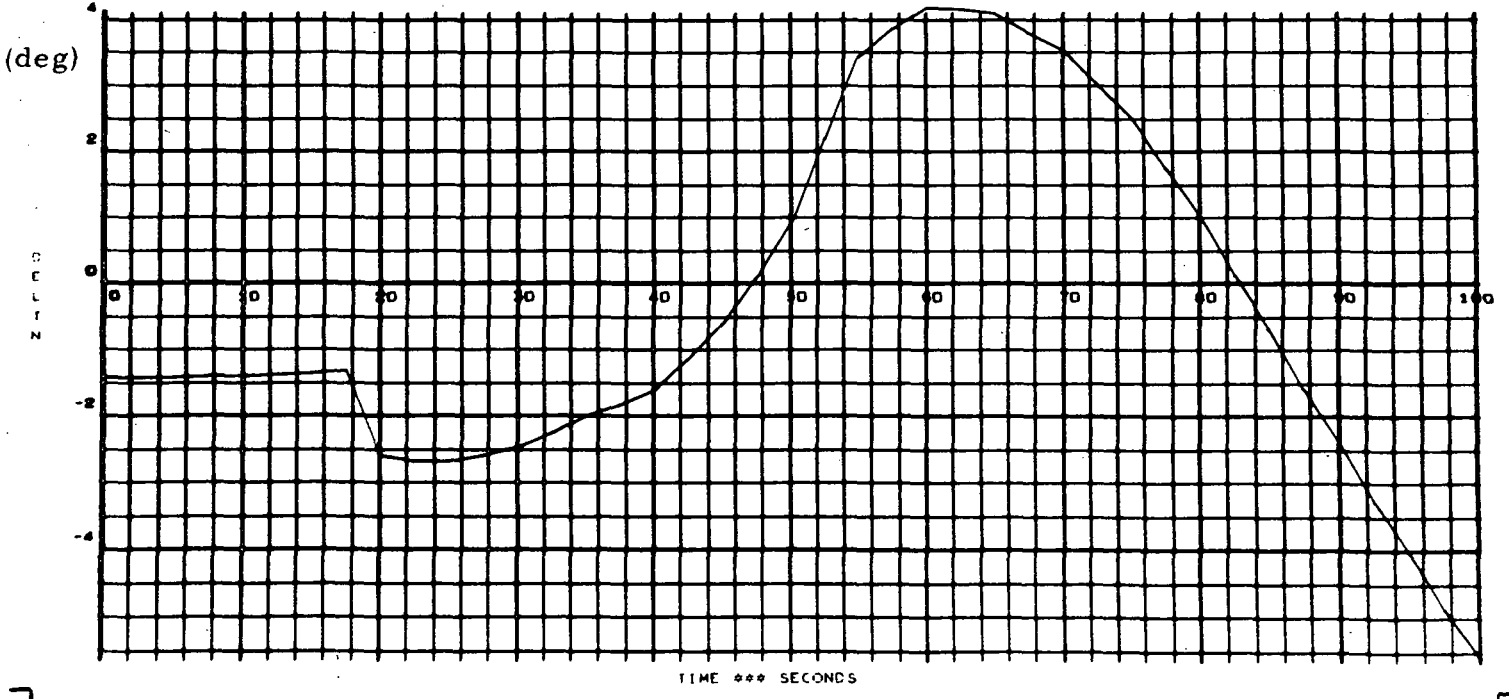
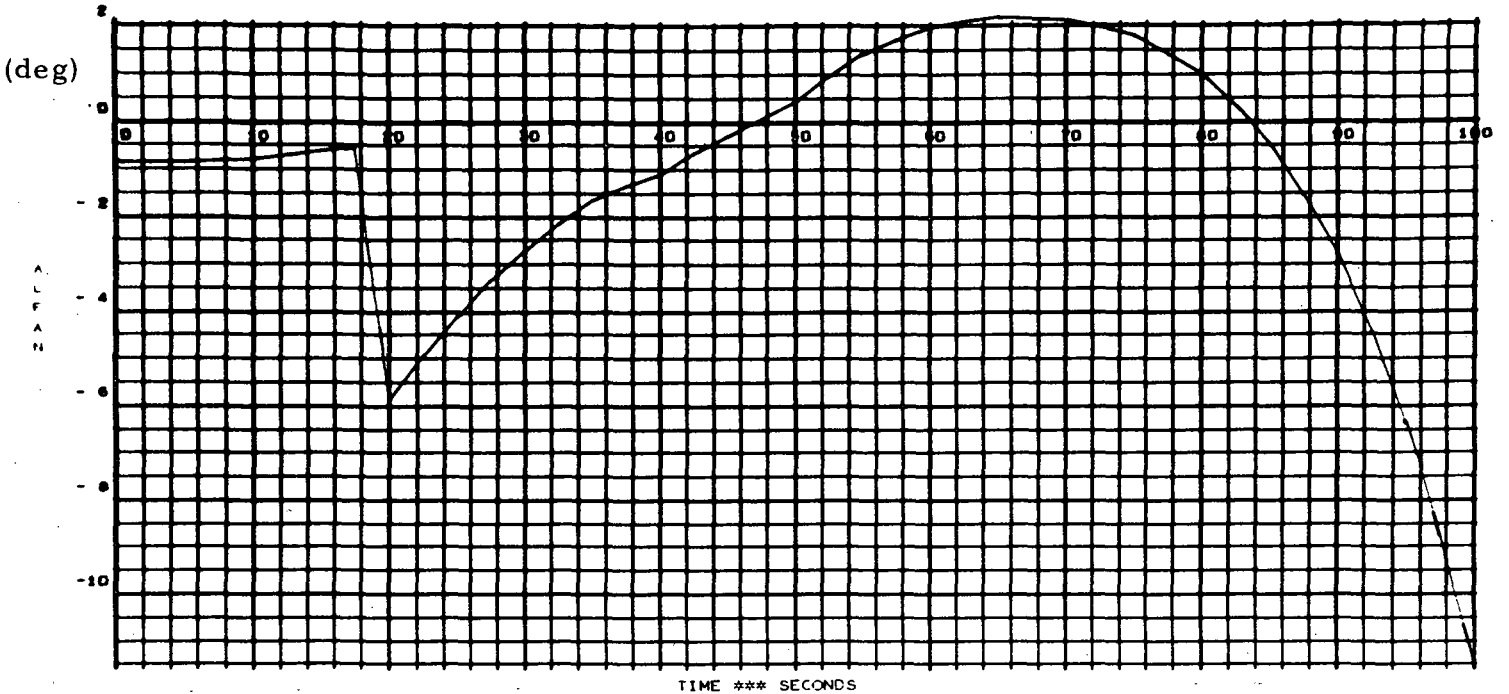


Fig. 2-9 - Trim Gimbal Angle $\delta\theta_0$ and Angle of Attack α_0 Computed by Simultaneous Solution of Trim EOM from Zero-Lift Trajectory Data Provided by MSFC, Aero-Astroynamics Laboratory, for MDAC Configuration 20

$$\frac{\partial P}{x(100 \text{ sec})} = -0.061 \frac{\text{kg}}{\text{m}} ; \quad \frac{\partial P}{|y(100 \text{ sec})|} = 0.027 \frac{\text{kg}}{\text{m}} ;$$

$$\frac{\partial P}{z(100 \text{ sec})} = 0.035 \frac{\text{kg}}{\text{in}} ; \quad \frac{\partial P}{\dot{x}(100 \text{ sec})} = -6.8 \frac{\text{kg}}{\text{m/sec}} ;$$

$$\frac{\partial P}{|\dot{y}(100 \text{ sec})|} = 0.43 \frac{\text{kg}}{\text{m/sec}} ; \quad \frac{\partial P}{\dot{z}(100 \text{ sec})} = 4.0 \frac{\text{kg}}{\text{m/sec}}$$

Section 3
OPTIMIZATION RESULTS

3.1 PITCH CONTROLLER DESIGN FOR MAXIMUM LOAD RELIEF BASED ON 2-DOF MODEL

In order to obtain a direct indication of control action related structural load reductions, it is necessary to compute representative loads during simulations. A simple form to approximate fuselage bending load perturbations was adopted from previous (wingless) symmetrical booster control practice (Ref. 3) in the early phase of this study.

$$\begin{aligned} \text{Bending Moment Indicator} &= \frac{M_B}{M'_\beta} (x) \\ &= R(x) (\alpha_o + \alpha) + \beta_o + \beta \end{aligned}$$

where

$$R(x) = \frac{M'_\alpha(x)}{M'_\beta(x)}$$

Based on approximate load distributions, $R(x)$ was calculated for the booster-orbiter rear attachment point for the configuration studied.

Since reduction of peak loads is of major concern to the designer, the most direct approach to accomplish this was to express the performance index in terms of the peak bending loads encountered in each simulation:

$$J = \max \left| \frac{M_B(\tau)}{M'_\beta} \right| \rightarrow \min$$

$$t_v \leq \tau \leq t_v + T$$

An additional term had to be included to limit sudden vehicle rotations in response to high wind shears and thus assure a sufficient amount of trajectory stability. A simple, yet effective, stability term is

$$J_s = \int_{t_v}^{t_v+T} |\dot{\phi}| dt$$

which was added to the basic load relief criterion. The complete load relief performance index which accounts for likely occurrence of either one of two adverse wind conditions then becomes:

$$J = \max_{\substack{i = \text{Wind A,} \\ \text{Wind B}}} \left\{ \max_{t \leq \tau \leq t_v + T} \frac{M_B(\tau)}{M'_\beta} + q \int_{t_v}^{t_v+T} |\dot{\phi}| dt \right\}_i$$

This criterion was applied to determine load relief control gain schedules for the MSFC space shuttle configuration described in Vol. II.

Two synthetic head wind profiles from Fig. 2-6 were used to represent adverse flight conditions and thus reduce the sensitivity of the optimal controller to off-nominal wind conditions.

Typical results are shown in Fig. 3-1, where loads and dynamic response of the optimized system to wind profile $\alpha_{wA}(t)$ are compared with a conventional constant gain controller. Likewise, in Fig. 3-2, optimized system response is compared with a constant gain case for a different headwind profile $\alpha_{wB}(t)$. A simple attitude error plus rate error feedback law was used in both cases.

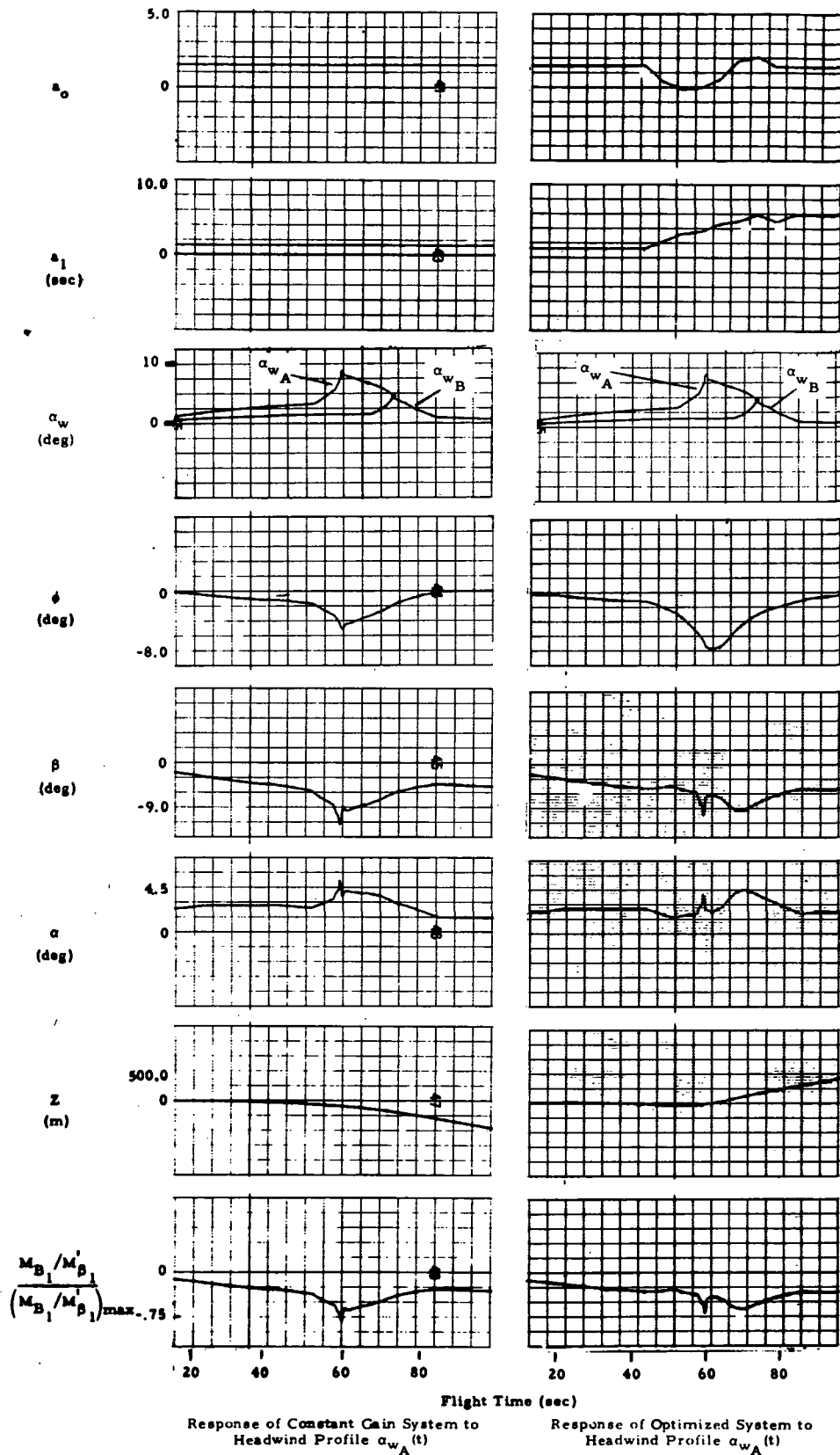


Fig. 3-1 - Optimized Simulations of the Composite MSFC Shuttle Considering Two Adverse Wind Profiles (Control gains are initialized at $a_0 = 1.5$, $a_1 = 1.5$ sec, and $g_2 = 0 \text{ deg/m}^2\text{sec}^2$, $a_{ii}(t)$ and $a_{11}(t)$ are optimized. Stability weighting term $q = 0.75$, look-ahead interval (T) is 15 sec and up-date interval is 5 sec.)

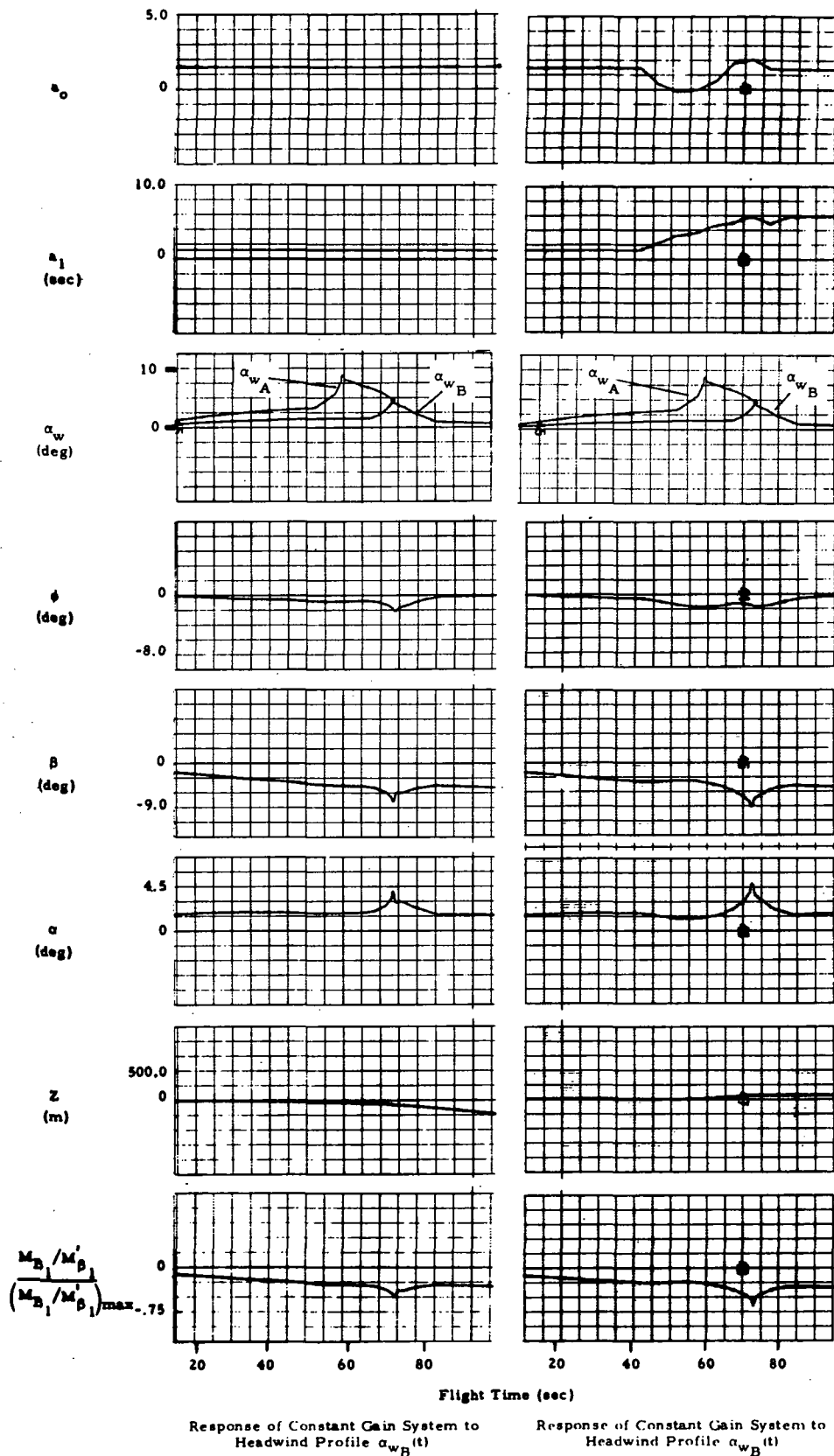


Fig. 3-2 - Optimized Simulations of the Composite MSFC Shuttle Considering Two Adverse Wind Profiles (Control gains are initialized at $a_0 = 1.5$, $a_1 = 1.5$ sec, and $R_2 = 0$ deg/m/sec². $a_0(t)$ and $a_1(t)$ are optimized. Stability weighting term $q = 0.75$, look-ahead interval (T) is 15 sec and up-date interval is 5 sec.)

The floating optimization interval was $T = 15$ sec. However, the optimization of gain slopes \dot{a}_0, \dot{a}_1 was updated every five seconds as indicated by the break points in the optimal gain schedules. The weighting term which was included to ensure sufficient trajectory stability was weighted by $q = 0.75$. In comparing the bending load histories at the bottom strips, it is easy to see that peak bending loads for both optimized cases were approximately the same. Bending due to α_{wA} (Fig. 3-1) was reduced from 0.83 to about 0.70, and bending due to α_{wB} (Fig. 3-2) was increased from 0.50 to about 0.70, thus verifying the tradeoff solution expected. Note verification of classical load relief attitude control technique in the shape of $a_0(t)$.

It was noticed that the single weighting term q could also be used to find the best controller to minimize lateral drift (z). Figures 3-3 and 3-4 verify this; note tradeoffs in bending and attitude errors between the lateral drift and the values of $q = 0.75, 0.96, \text{ and } 1.5$, respectively.

3.2 PITCH CONTROLLER DESIGN FOR MAXIMUM LOAD RELIEF BASED ON 6-DOF MODEL

Shuttle ascent dynamics were expanded from the simple pitch-plane model to full six-degree-of-freedom dynamics. Checkout and initial optimizations were again performed on the pitch plane for the two adverse headwinds α_{wA}, α_{wB} . Initial results are shown in Fig. 3-5. These results confirmed those of the simplified pitch plane study with minor differences attributed to configuration changes (MDAC-20 was used instead of MSFC configuration in the initial study) and nominal trajectory differences. Again, a near perfect tradeoff was accomplished for the peak bending loads; i.e., a reduction of the bending load indicator from 0.75 to 0.39 for Wind A and a decrease from 0.45 to 0.39 for Wind B.

It is interesting to note that the optimized attitude gain schedule calls for negative a_0 during the time of high dynamic pressure. This causes engine deflections which increase the rotation into the wind, thus reducing bending loads. Due to the high aerodynamic stability of this winged configuration, rotational stability is not jeopardized by this maneuver.

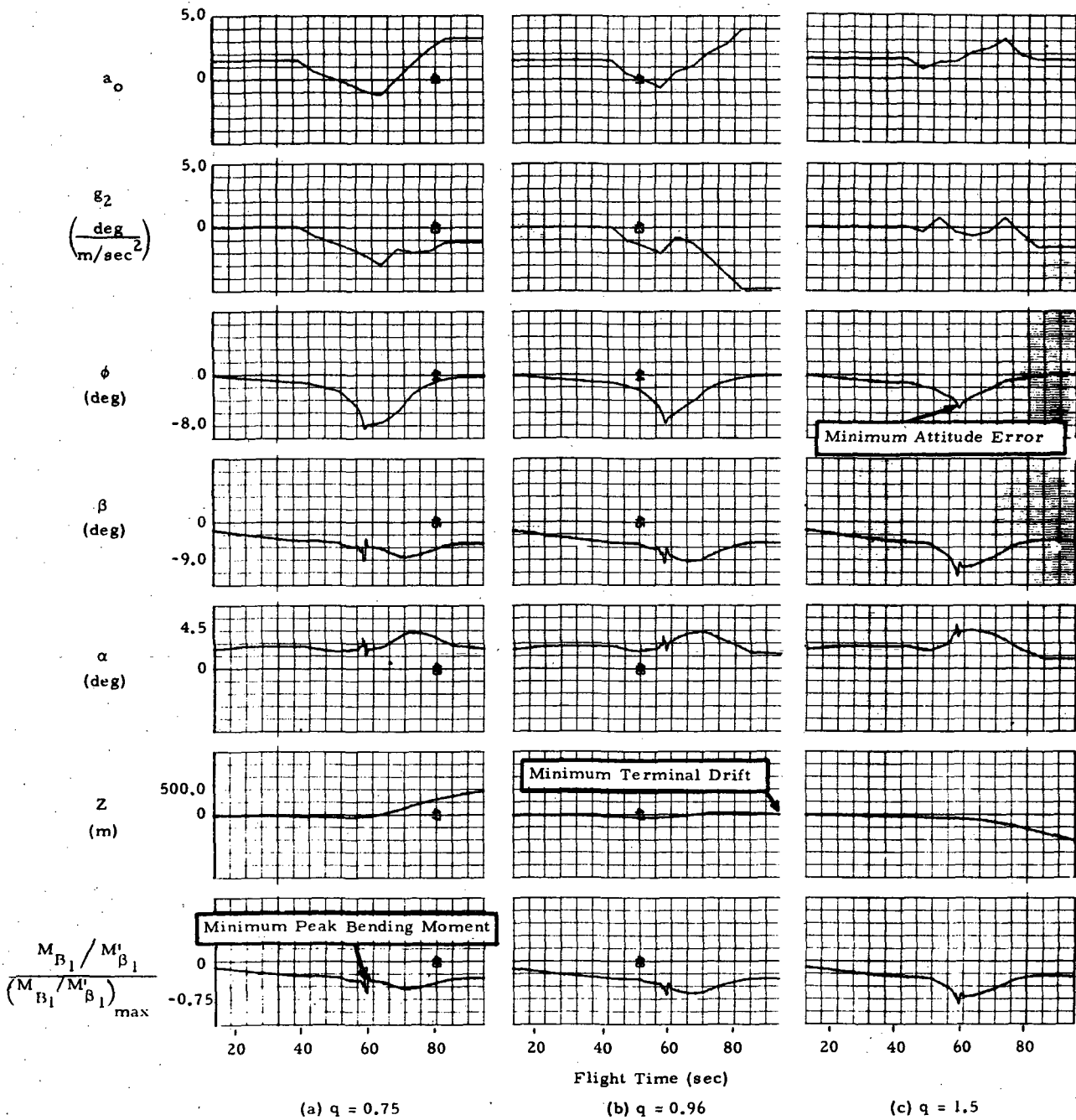


Fig. 3-3 - Optimized Simulations of the Composite MSFC Shuttle for Variation in q (stability weighting term in performance index). (Considering two adverse wind profiles (peak wind and gust) at 60 sec and 74 sec, respectively, with response to 60 sec wind and gust peak being shown. Control gains are initialized at $a_0 = 1.5$, $a_1 = 1.5$ sec, whereas $a_0(t)$ and $g_2(t)$ are optimized. Look-ahead interval (T) is 15 sec, and up-date interval between change in gain schedule slope changes is 5 sec.)

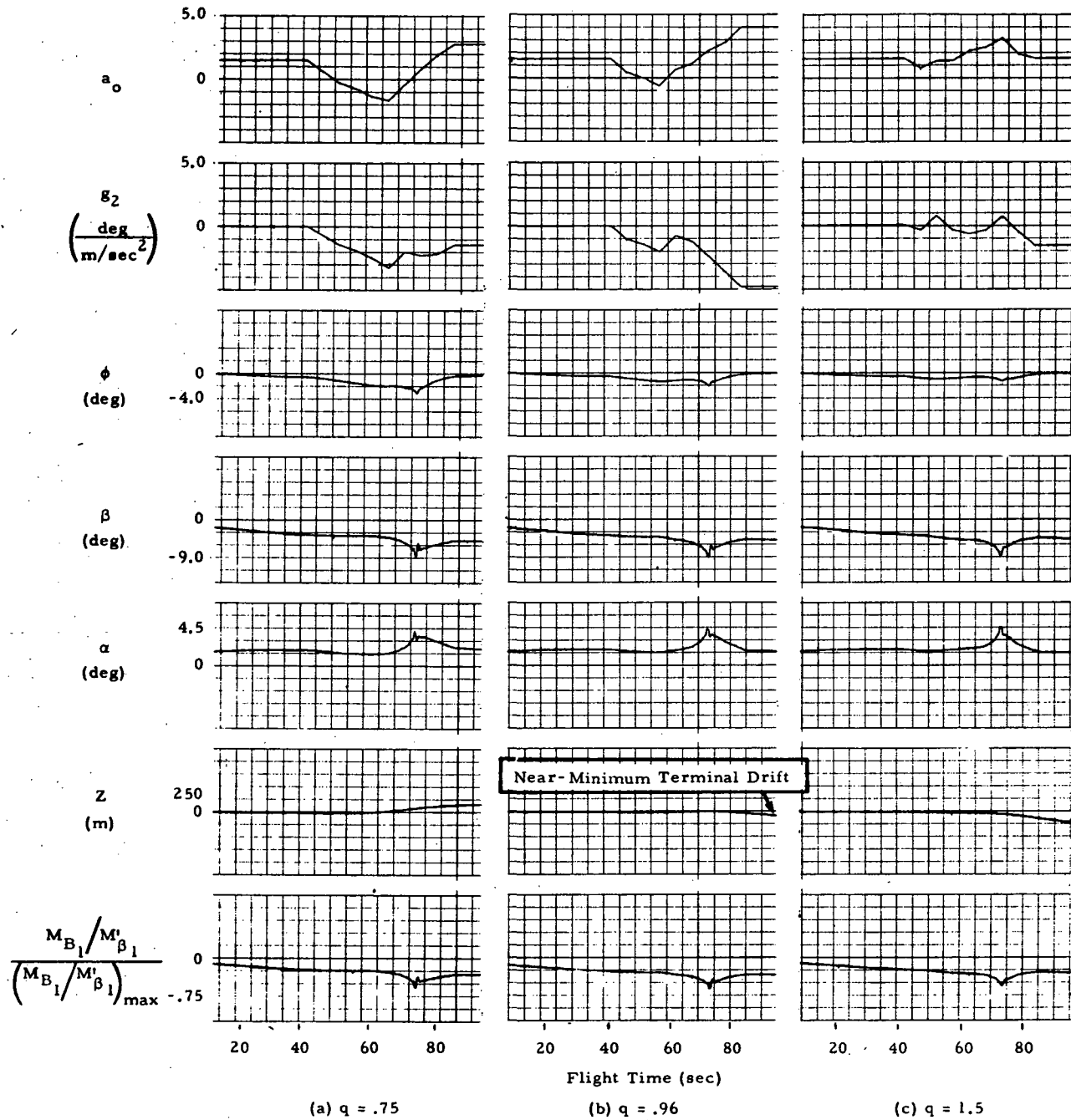
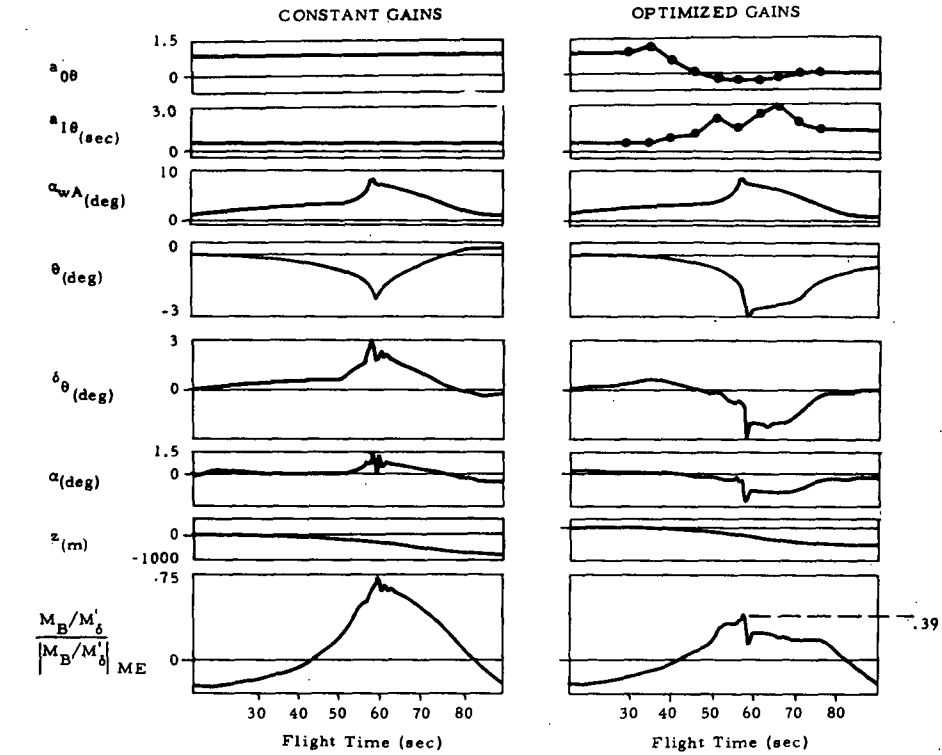
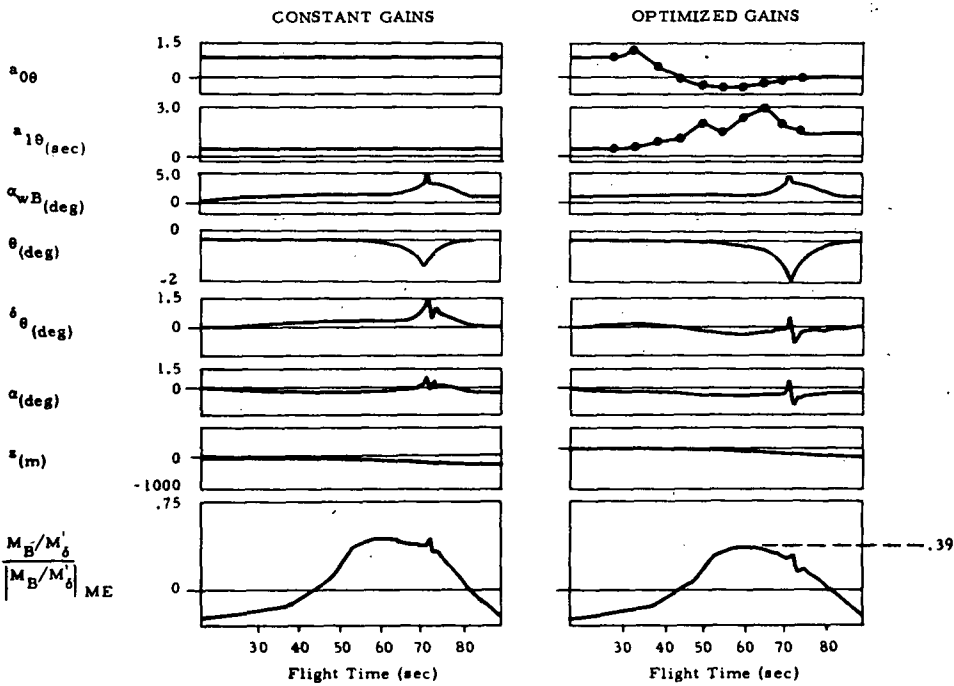


Fig. 3-4 - Optimized Simulations of the Composite MSFC Shuttle for Variation in q (stability weighting term in performance index). (Considering two adverse wind profiles (peak wind and gust) at 60 sec and 74 sec, respectively, with response to 74 sec peak being shown. Control gains are initialized at $a_0 = 1.5$, $a_1 = 1.5$ sec, whereas $a_0(t)$ and $g_2(t)$ are optimized. Look-ahead interval (T) is 15 sec, and up-date interval between change in gain schedule slope changes is 5 sec.)



A Response to Wind A (max. shear plus gust at max q)



B Response to Wind B (max. shear plus gust at Mach 2)

NOTE: Subscript "ME" denotes maximum expected value.

Fig. 3-5 - Pitch Control Gain Optimization for Maximum Load Relief for MDAC-20 Space Shuttle Configuration Using Performance Criterion (J) with Floating Optimization Interval $T = 15$ sec Stability Weighting Factor $q = 0.75$

3.3 YAW CONTROLLER DESIGN FOR MAXIMUM LOAD RELIEF

In order to gain a first insight into the yaw-roll control characteristics and into the trends of load relief yaw control system design, the same space shuttle configuration (MDAC-20) was subjected to severe side wind disturbances. The wind profiles A and B used previously as head winds were now assumed to act as side winds from 90 degrees to the pilot's right. Realistic data on structural loads due to side winds were not yet generated at the start of this study phase. Therefore, the bending load indicator derived to approximate booster bending loads about the pitch axis was also used to indicate bending loads about the yaw axis. Since this approach represents an oversimplification of rather complex structural and aerodynamic interactions, the results obtained are not meaningful for design purposes. However, this initial study of the yaw-roll problem allowed for a thorough checkout of the 6-DOF simulation and of the simulation-optimization interface. The erroneous bending load indicator drives yaw gains up, whereas later studies (described in Section 3.5) which use a realistic performance measure based on detailed structural analysis call for yaw attitude gain reductions to improve performance.

The misleading initial results are reported here to demonstrate the need and merits of developing design-related performance criteria for control system optimization. The substantial reductions in yaw-error obtained by the "optimized" system (Figs. 3-6 and 3-7) are later found to be the wrong design objective when physically meaningful performance criteria are used as shown in Fig. 3-15 of Section 3.5.

3.4 PITCH CONTROLLER DESIGN FOR MAXIMUM PAYLOAD

3.4.1 Formulation of Payload-Optimal Performance Criteria

The classical approaches to launch vehicle control require engineering tradeoffs between load relief and trajectory performance (Ref. 8). If loads are reduced to such an extent that lateral drift requires a large amount of extra

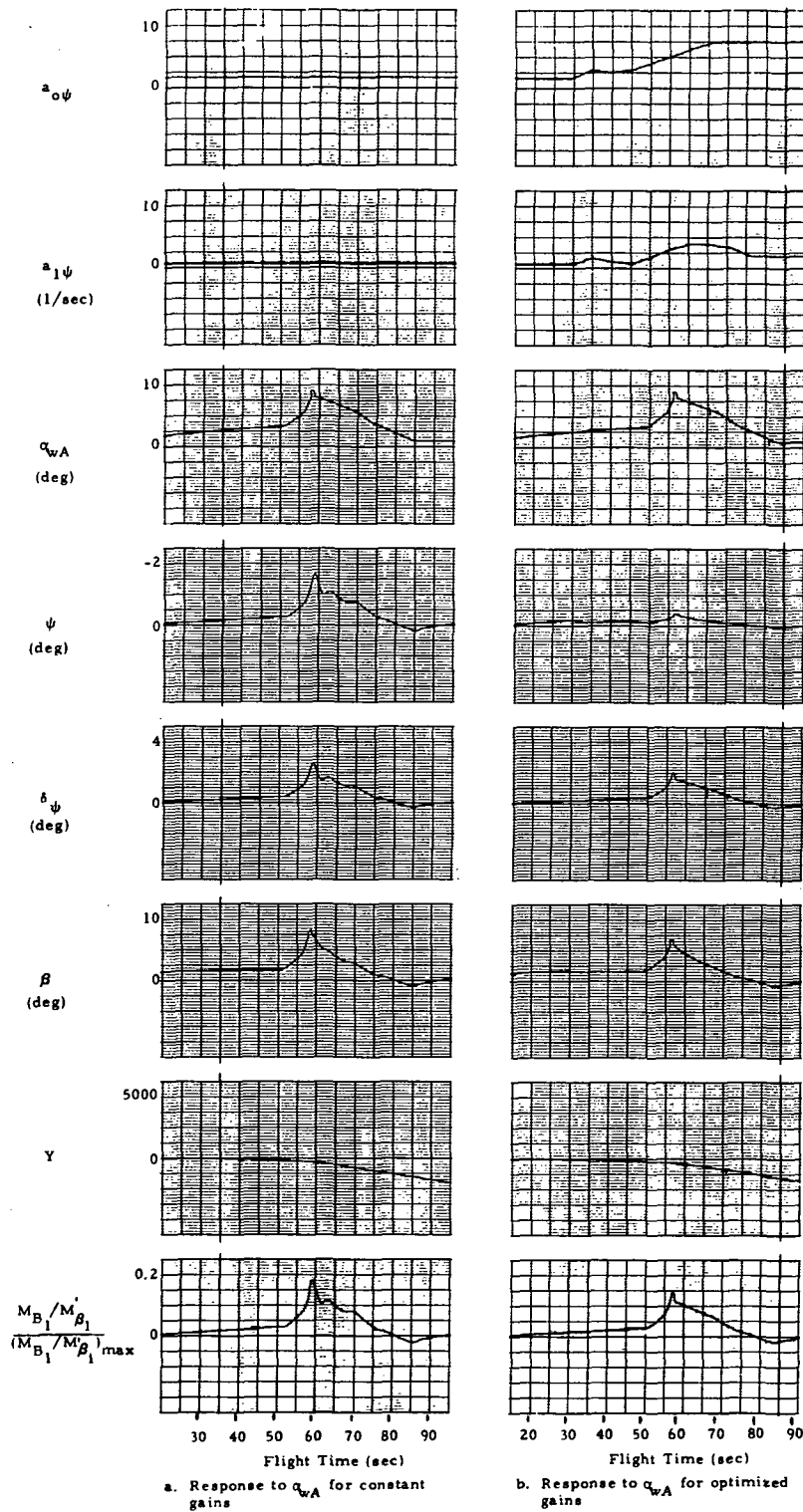


Fig. 3-6 - Initial Results for the Optimization of Yaw-Plane Control Gains for the MDAC Shuttle Configuration 20 Ascent Phase. (Optimization considered the possible occurrence of one of two MSFC synthetic wind profiles of Fig. 2-6. The stability weighting factor q was equal to zero with $a_{0\psi}$ and $a_{1\psi}$ initially 1.5 and 0.5, respectively, with optimization beginning at 30 sec and ending at 75 sec. Roll gains $a_{0\phi}$ and $a_{1\phi}$ are constant at 5.0 and 2.0, respectively. Results illustrated are responses to α_{WA} acting from 90 deg to the pilot's right.)

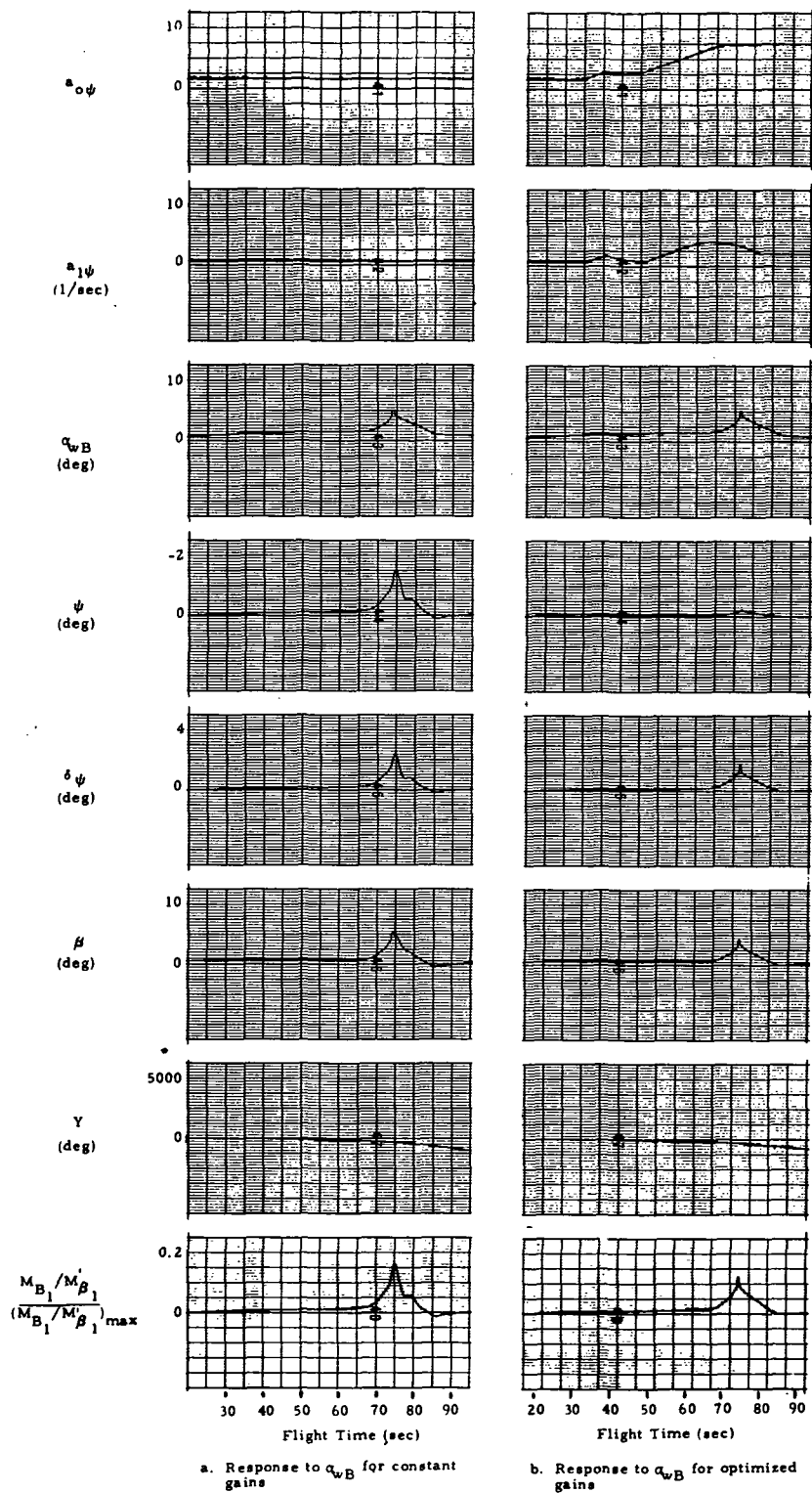


Fig. 3-7 - Initial Results for the Optimization of Yaw-Plane Control Gains for the MDAC Shuttle Configuration 20 Ascent Phase. (Optimization considered the possible occurrence of one of two MSFC synthetic wind profiles of Fig. 2-6. The stability weighting factor q was equal to zero with $a_{0\psi}$ and $a_{1\psi}$ initially 1.5 and 0.5, respectively, with optimization beginning at 30 sec and ending at 75 sec. Roll gains $a_{0\phi}$ and $a_{1\phi}$ are constant at 5.0 and 2.0, respectively. Results illustrated are responses to q_{wB} acting from 90 deg to the pilot's right.)

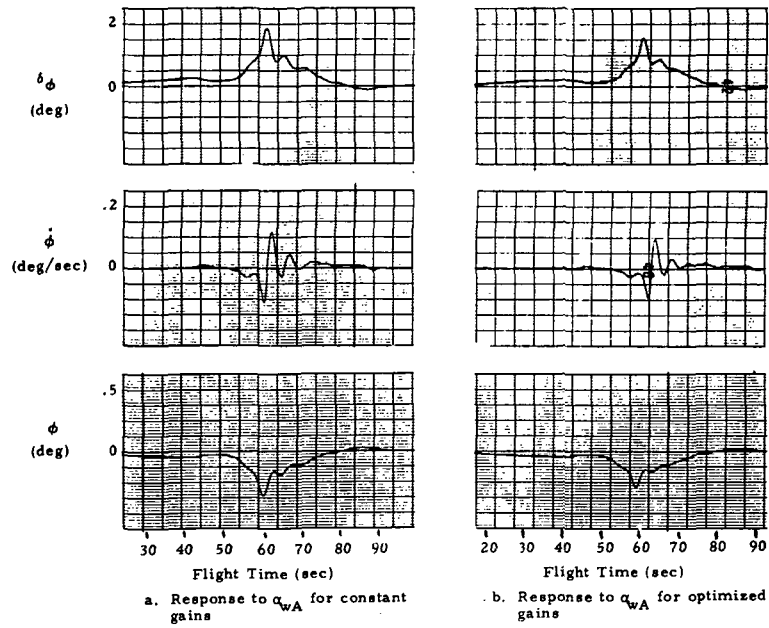


Fig. 3-7 (Continued)

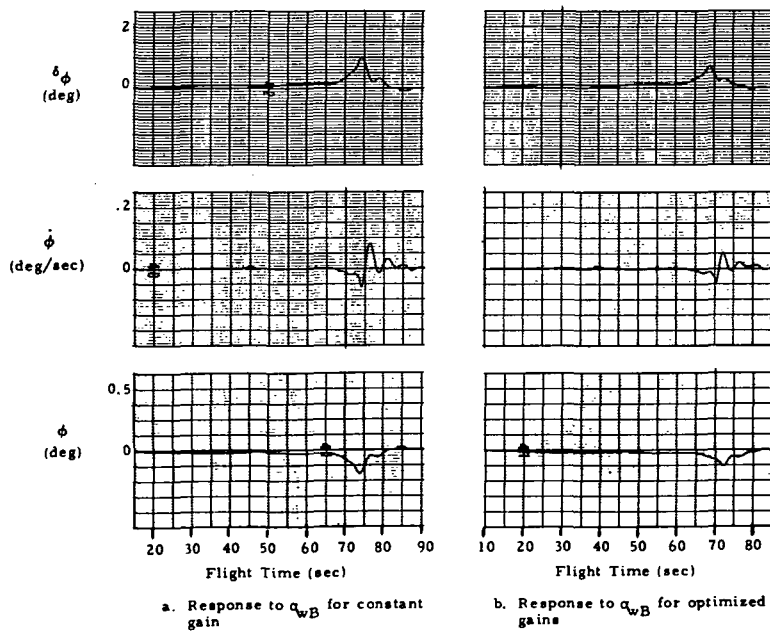


Fig. 3-8 (Continued)

propellant for flight path corrections, the savings in structural weight may be completely offset by these drift-related fuel penalties. The extreme sensitivity of vehicle economy to vehicle weight for reusable space shuttle configurations makes it necessary to consider additional factors in these trade-offs such as maximum gimbal angle and aerodynamic control surface deflections during powered ascent and their impact on orbit insertion weight. This large number of conflicting design factors make it highly desirable to relieve the engineer from tedious parametric studies by providing him with a systematic computer-aided design tool that relates all major flight characteristics such as peak structural loads, peak engine gimbal angles, peak hinge moments, and peak trajectory errors to orbit insertion weight or payload. The virtually free choice in formulating performance criteria combined with the realism of dynamic simulations makes the present hybrid optimization technique ideally suited to solve this problem of payload-optimal control system design.

For the computerized design of payload-optimal ascent control systems, it is necessary to derive payload sensitivities of all flight characteristics affected by attitude control dynamics.

The following performance index comprises the major payload penalties which depend upon flight control system performance:

$$\begin{aligned}
 J' = & \sum_{i=1}^6 \frac{\partial P}{\partial R_i} \left| R_{i_{\max}} - R_{i_0} \right| + \sum_{j=1}^3 \frac{\partial P}{\partial \delta_j} \left| \delta_{j_{\max}} - \delta_{j_0} \right| \\
 & + \sum_{m=1}^3 \left[\frac{\partial P}{\partial x_m} x_{m_{\max}} + \frac{\partial P}{\partial v_m} v_{m_{\max}} \right] \\
 & + \frac{\partial P}{\partial H_M} \left| H_{M_{\max}} \right|
 \end{aligned}$$

where

- P = payload penalty or decrease
- R_i = forces at the booster-orbiter interface
- δ_i = main booster engine gimbal angles for roll, pitch, yaw control including δ_{trim}
- x_m = deviations from reference trajectory in x, y, z direction
- v_m = velocity errors with respect to reference trajectory in x, y, z direction
- H_M = hinge moment due to aerodynamic surface deflection

The subscript "o" denotes design values corresponding to the nominal payload capability.

The design goal of maximum payload can then be achieved by minimization of this payload penalty functional J' .

In order to avoid excessive angular rates by the vehicle in response to gust-type wind disturbances, an additional cost functional was formulated:

$$J'' = \frac{1}{T} \int_t^{t+T} \left[\left| \frac{\dot{\phi}}{\dot{\phi}_{ME}} \right| + q_{\dot{\theta}} \left| \frac{\dot{\theta}}{\dot{\theta}_{ME}} \right| + q_{\dot{\psi}} \left| \frac{\dot{\psi}}{\dot{\psi}_{ME}} \right| \right] dt$$

where $\dot{\phi}$, $\dot{\theta}$, $\dot{\psi}$, are the roll, pitch, and yaw rates, respectively, and the subscript "ME" denotes maximum expected values. $q_{\dot{\theta}}$ and $q_{\dot{\psi}}$ are weighting coefficients reflecting the design constraints imposed on the various vehicle rates. J'' should be kept small to assure smooth flying qualities. The criteria (J) and (J'') can be readily combined into a single performance criterion

$$J = J' + qJ'' \rightarrow \min.$$

which makes possible the minimization of all payload penalties while a weighted flying quality criterion qJ'' is simultaneously satisfied.

All three weighting factors (q , $q_{\dot{\theta}}$, $q_{\dot{\psi}}$) are directly related to well-established design guidelines concerning admissible angular rates and therefore easy to adjust after a small number of trial optimizations.

This is a major advantage over quadratic form J functionals, where a large number of weighting factors with little or no physical meaning must be selected by trial and error.

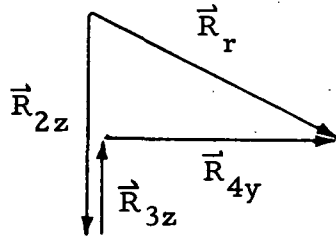
3.4.2 Application to Pitch Controller Design

Figure 3-10 shows pitch plane results for α_{wA} where this new J function for maximizing payload was implemented. The structural loads at the booster/orbiter rear attachment points were found to have the strongest impact on structural weight requirements and associated payload penalties. As shown in Volume II, the dynamic simulation was extended to generate time histories of all major terms in this new payload-related performance measure. Peak values $R_{i_{max}}$, $\delta_{j_{max}}$, ... , are sampled during simulation and transferred to the performance analyzer at the end of each run. The interface geometry and notations are shown in Fig. 3-11. The major payload penalty term

$$\frac{\partial P}{\partial R_r} (R_{r_{max}} - R_{r_o}) = \Delta P_R$$

is associated with the resultant force R_r ,

$$R_r = \sqrt{(R_{2z} + R_{3z})^2 + R_{4y}^2}$$



which is the vector sum of \vec{R}_{2z} , \vec{R}_{3z} and \vec{R}_{4y} . In the absence of sidewinds and lateral motion (yaw, roll, sideslip), \vec{R}_r acts in the z -direction of the

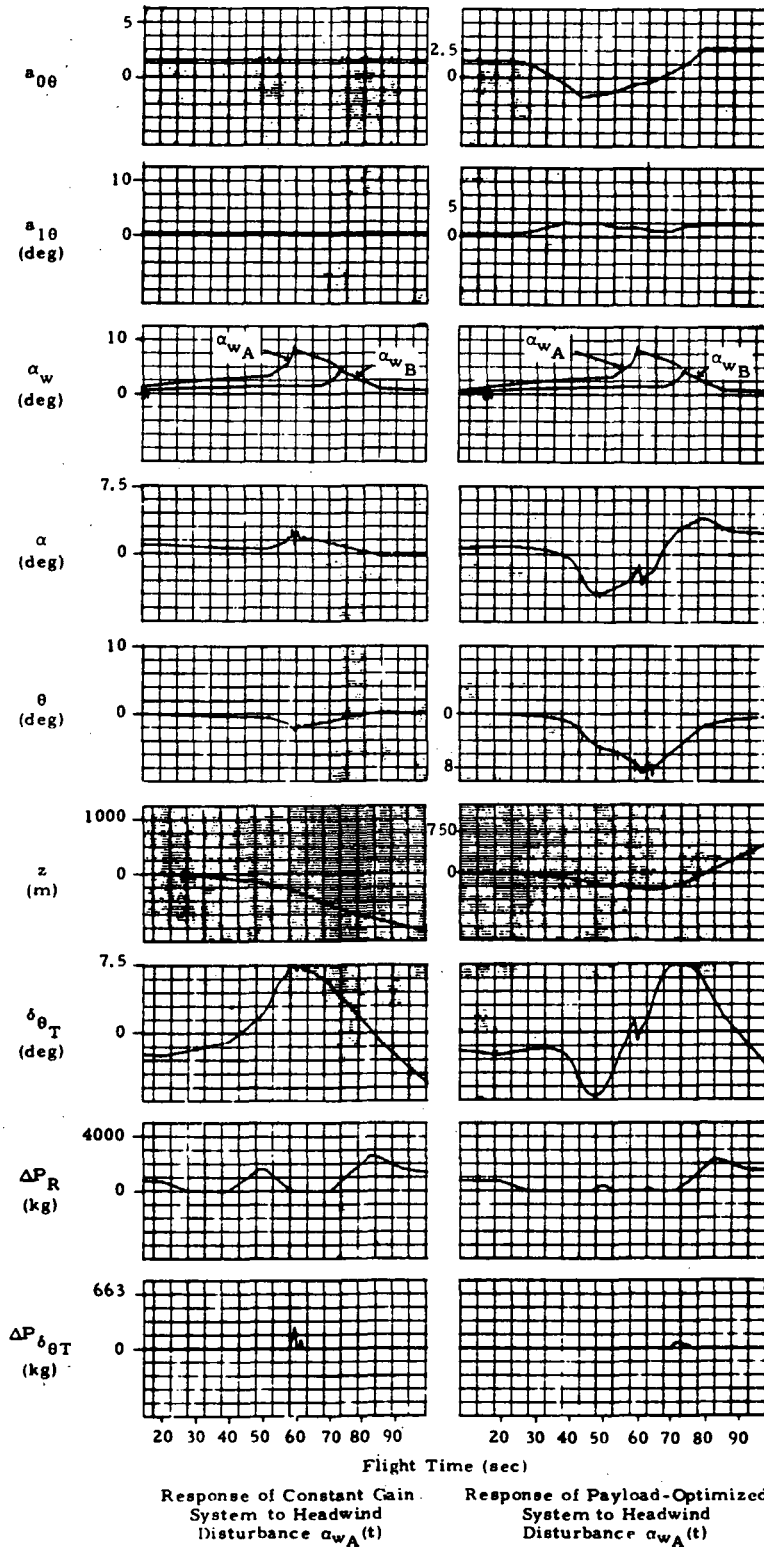


Fig. 3-10 - Optimization of Pitch Control Gain Schedules for Maximum Payload. Vehicle is subjected to two severe headwind disturbances (A or B of Fig. 2-6) during optimization.

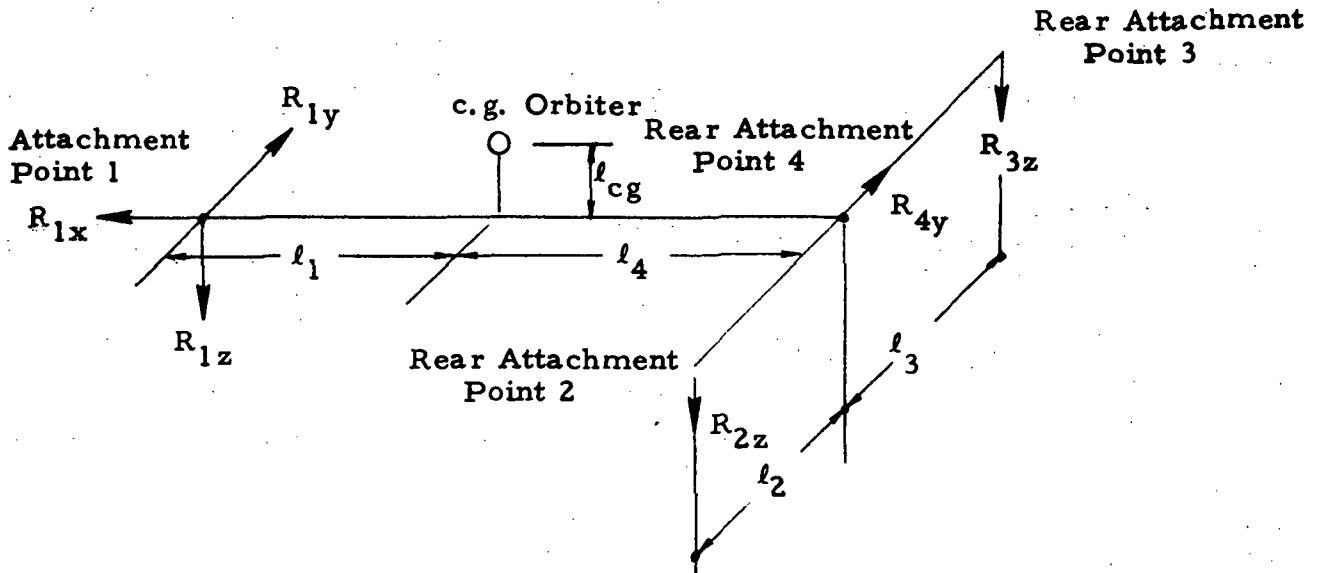


Fig. 3-11 - Components of Interface Forces and Geometry of the Attachment Points of Shuttle Booster and Orbiter (MDAC-20 Configuration)

vehicle. In general, however, \vec{R}_R acts slightly out of the pitch plane. The nominal design value for this load was assumed to be

$$|R_{R_o}| = 4 \times 10^5 \text{ N}$$

Only loads in excess of R_{R_o} were therefore accounted for in determining associated payload penalties.

The second largest effect on payload is due to maximum engine gimbal angle requirements for pitch plane deflections as required for pitch and roll corrections. It was assumed that the vehicle design was based on

$$|\delta\theta_{T_o}| \leq 7^\circ$$

gimbal angle requirement. Engine deflections in excess of 7 degrees were therefore accounted for in determining the payload penalty

$$\frac{\partial P}{\partial \delta_{\theta T}} \left(\left| \delta_{\theta T \max} \right| - \left| \delta_{\theta T 0} \right| \right) \equiv \Delta P_{\delta_{\theta}}$$

Time histories of these two major payload penalties (ΔP_R and $\Delta P_{\delta_{\theta T}}$) are therefore included in all subsequent recordings of vehicle response.

Typical results are shown in Fig. 3-10, which shows responses to headwind profile $\alpha_{wA}(t)$. Figure 3-12 shows responses to the other headwind profile $\alpha_{wB}(t)$. The optimization was again based on the assumption that one of the two adverse disturbances (A or B) is likely to occur.

The optimized gain schedules call for even more rotation into the wind by large negative attitude gains a_{θ} in the region of high dynamic pressure. This causes a substantial reduction in structural load related payload penalties for the most severe wind condition A by 1400 kg in the region of high q around $t=50$ sec, as recorded in Fig. 3-10. Engine gimbal requirements are held within 7 degrees. These improvements are overshadowed by a higher payload penalty later in the flight, peaking at 82 seconds. This latter peak, beyond the max q -region, proved to be almost insensitive to changes in the control gains. A detailed analysis revealed that cg tracking problems associated with this configuration in combination with the specified zero-lift trajectory are responsible for these high loads late in the ascent.

From the standpoint of payload maximization, minor changes in the trajectory and/or cg-locations of orbiter and booster would appear attractive for this configuration. Then, the payload gains due to the optimized controller adjustments in the high- q region could be realized.

This example demonstrates that information about design problems and potential improvements can be gained early in the development of complex vehicles by this control system design technique.

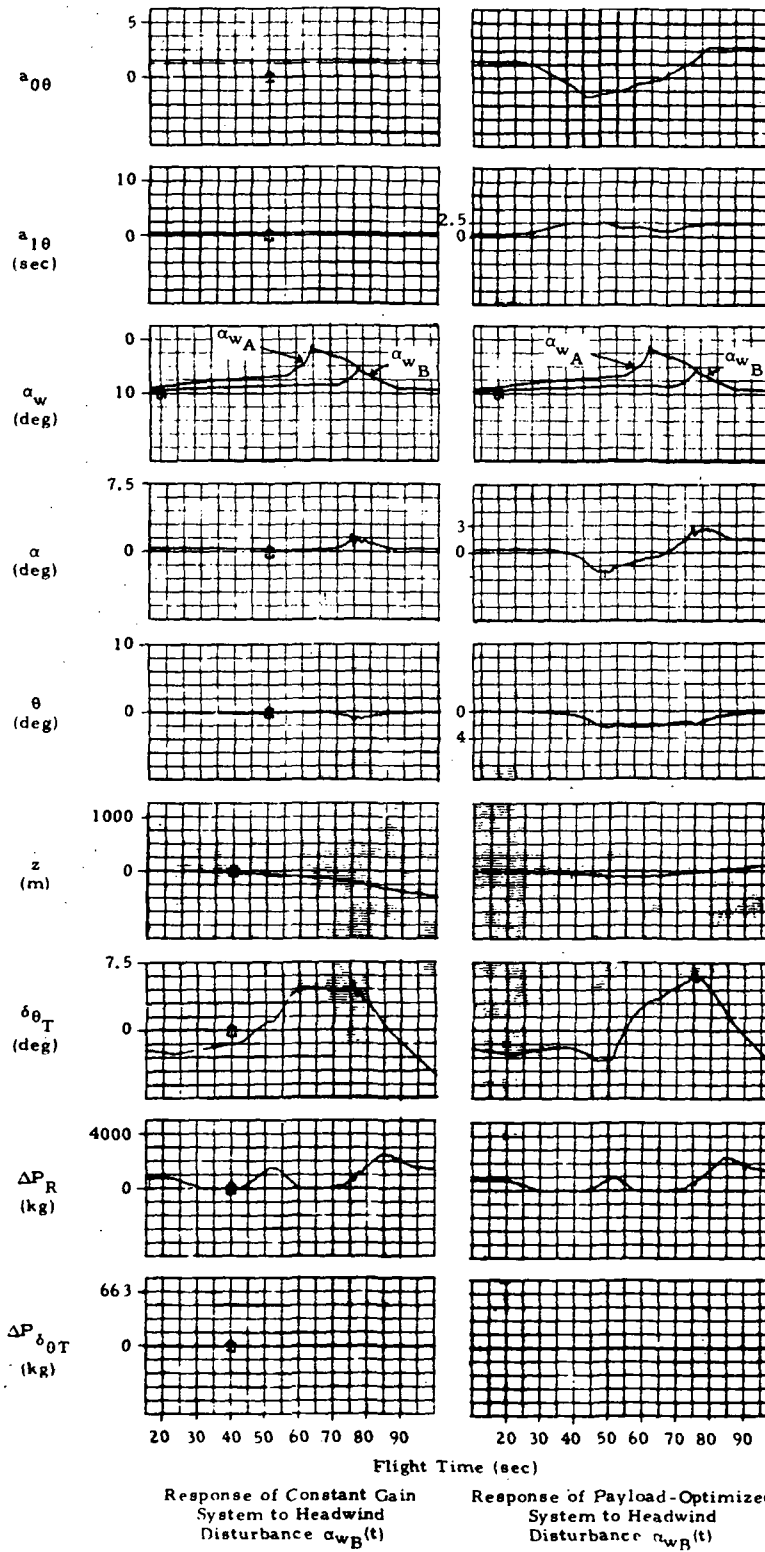


Fig. 3-12 - Performance of Constant Gain and Optimized Systems to Headwind Profile B (of Fig. 2-6)

The strong dependence of payload penalties on attitude gain schedules during high dynamic pressure is further evidenced by the plots of Figs. 3-13 and 3-14. The payload penalty surfaces vary strongly with changes in $\dot{a}_{0\theta}$, but very little, if any, with changes in rate gain slopes $\dot{a}_{1\theta}$. Such findings early in the design of advanced space vehicle controllers may be used in the future to keep certain gains constant which would speed up the iterative search for the remaining gain schedules without much loss in optimality.

3.5 YAW CONTROLLER DESIGN FOR MAXIMUM PAYLOAD

Figures 3-15 and 3-16 show the initial results for optimization of the yaw controller in order to achieve maximum payload. The same two winds used in all previous studies were used as sidewinds (90° from pilot's right) to perform this optimization.

The flying quality term in the performance index was modified to limit sideslip (β).

$$J'' = q \int \left[q_{\beta} |\beta| + q_{\dot{\psi}} |\dot{\psi}| + q_{\dot{\phi}} |\dot{\phi}| \right] dt$$

The controller gains optimized were yaw position feedback ($a_{0\psi}$) and sideslip angle feedback ($b_{0\psi}$). The objective here was to limit roll (ϕ) and sideslip (β) while minimizing all major payload penalties (ΔP) affected by the flight control system. This objective was achieved, sideslip (β) was reduced from about 5 degrees to about 1 degree, lateral drift was reduced by 50%, and payload penalties due to structural loads (ΔP_R) were reduced by 1800 kg for the worst wind case $\alpha_{wA}(t)$. The engine deflection (δ_{ϕ}) was reduced by 75% which is desirable since δ_{ϕ} adds to the total gimbal requirements for pitch and roll which can become critical under severe sidewinds.

A near perfect tradeoff was obtained in the reductions of the payload penalty to $\Delta P_R \approx 1200$ kg for both winds, whereas Wind A would cause a 3000 kg penalty for the constant gain system. Both cases yield decreased

	$\dot{a}_{0\theta}$	$\dot{a}_{1\theta}$
Grid Search Minimum	-0.1800 sec^{-1}	0.0000
Final Gradient Minimum	-0.1761 sec^{-1}	+0.0341

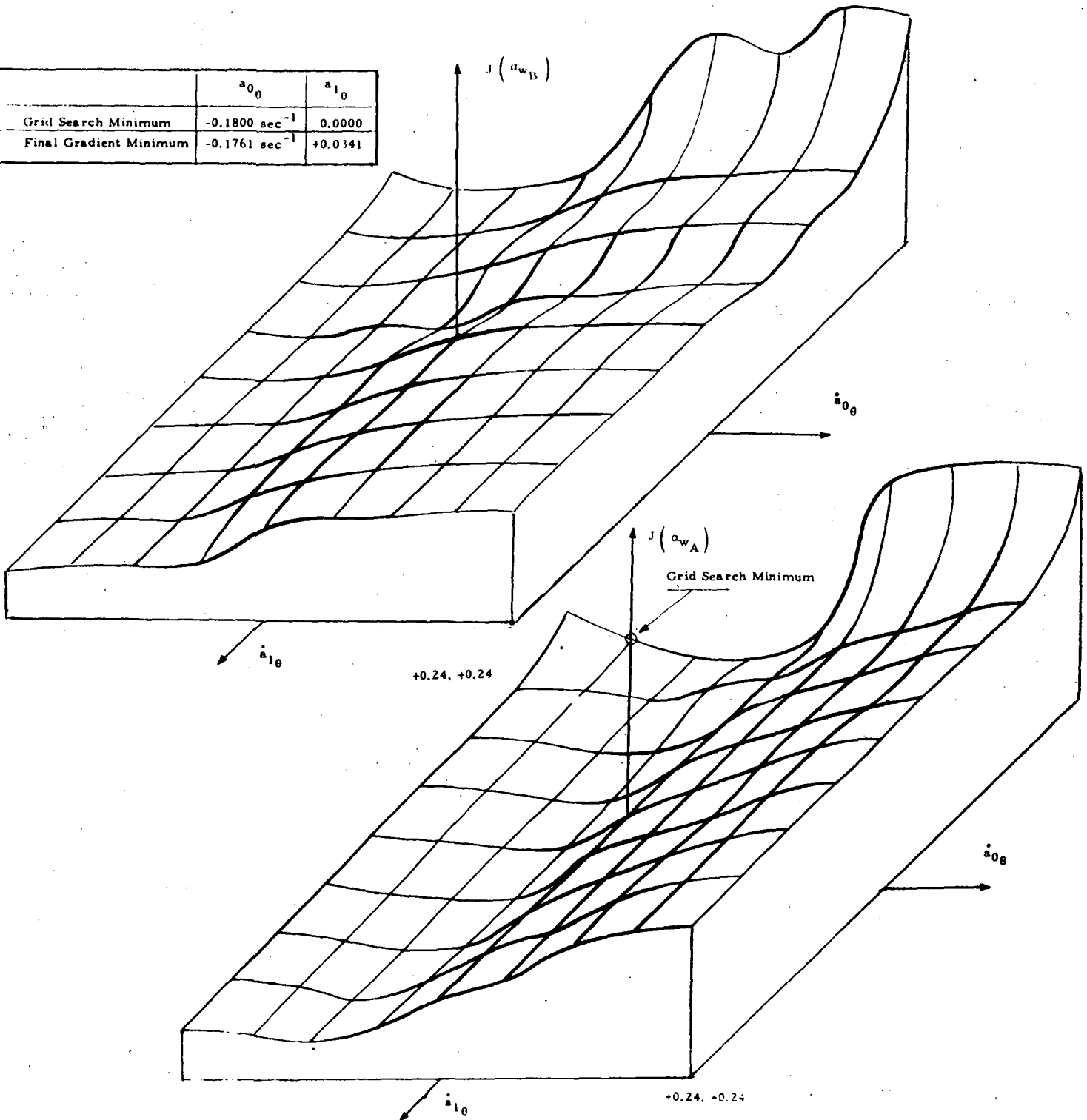


Fig. 3-13 - Payload Penalty Surfaces as Functions of Pitch Control Gain Slopes $\dot{a}_{0\theta}$ and $\dot{a}_{1\theta}$ Generated by Grid Search Varying $\dot{a}_{0\theta}$ Systematically from -0.24 to +0.24 sec^{-1} and $\dot{a}_{1\theta}$ from -0.24 to +0.24. Optimization interval reaches from time 37.5 sec to 57.5 sec of the case shown in Figs. 3-10 and 3-12. This includes first interface load peak at 52.5 seconds.

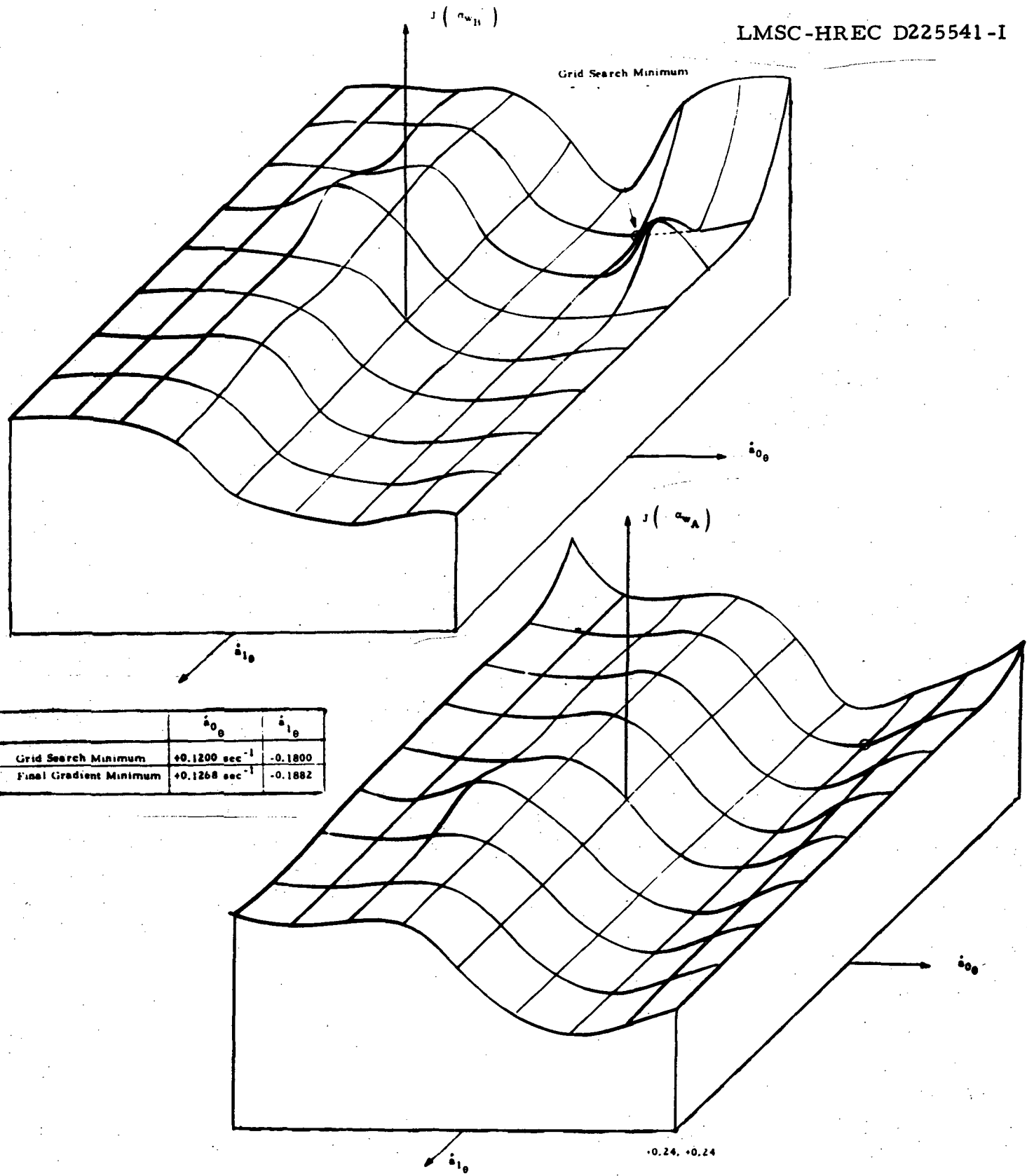


Fig. 3-14 - Payload Penalty Surfaces as Functions of Pitch Control Gain Slopes $\dot{\alpha}_{0\theta}$ and $\dot{\alpha}_{1\theta}$ at a Later Optimization Interval $57.5 \text{ sec} \leq t \leq 77.5 \text{ sec}$ of the Case Shown in Figs. 3-10 and 3-12. Interval now includes peaks of both winds at 60 and 75 seconds.

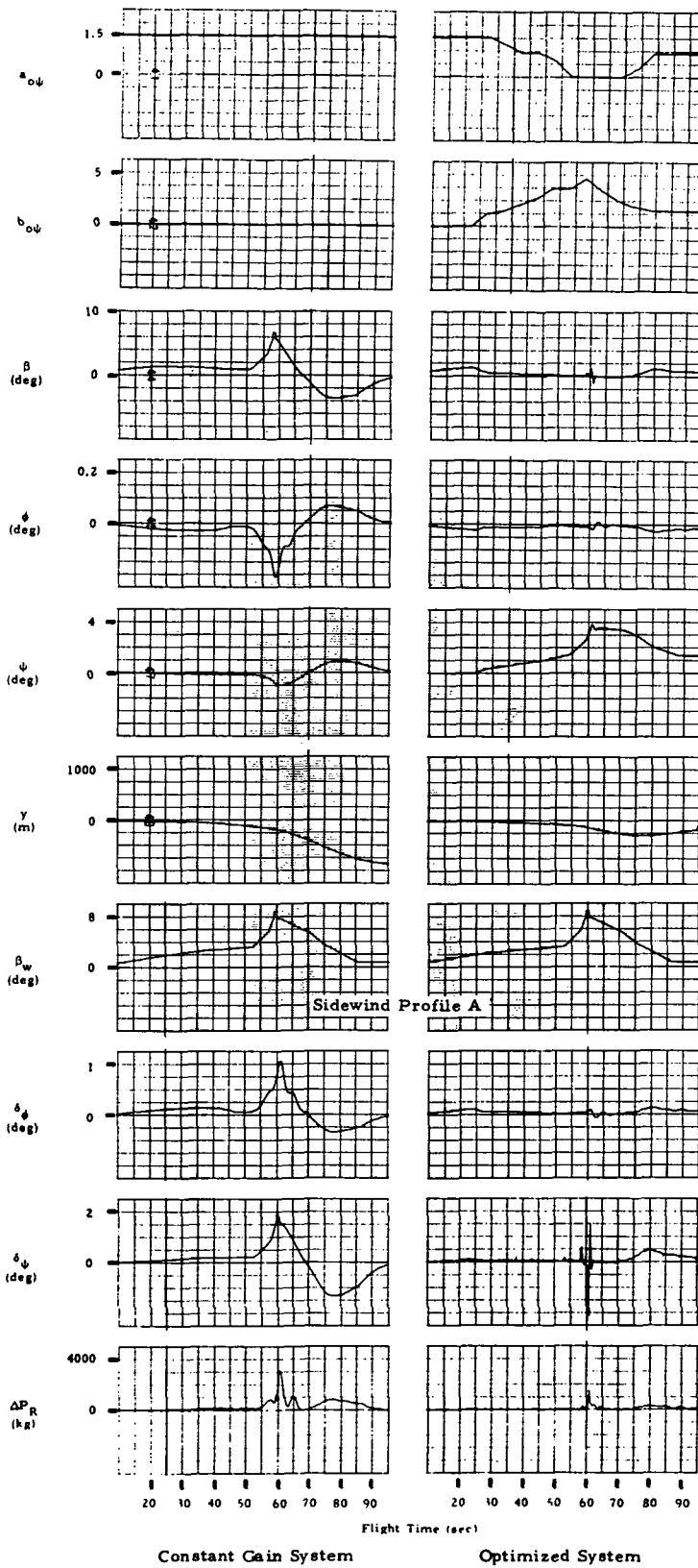


Fig. 3-15 - Optimization of Yaw Control Gain Schedules for Maximum Payload. Vehicle is subjected to two adverse sidewind disturbances (A or B) during optimization.

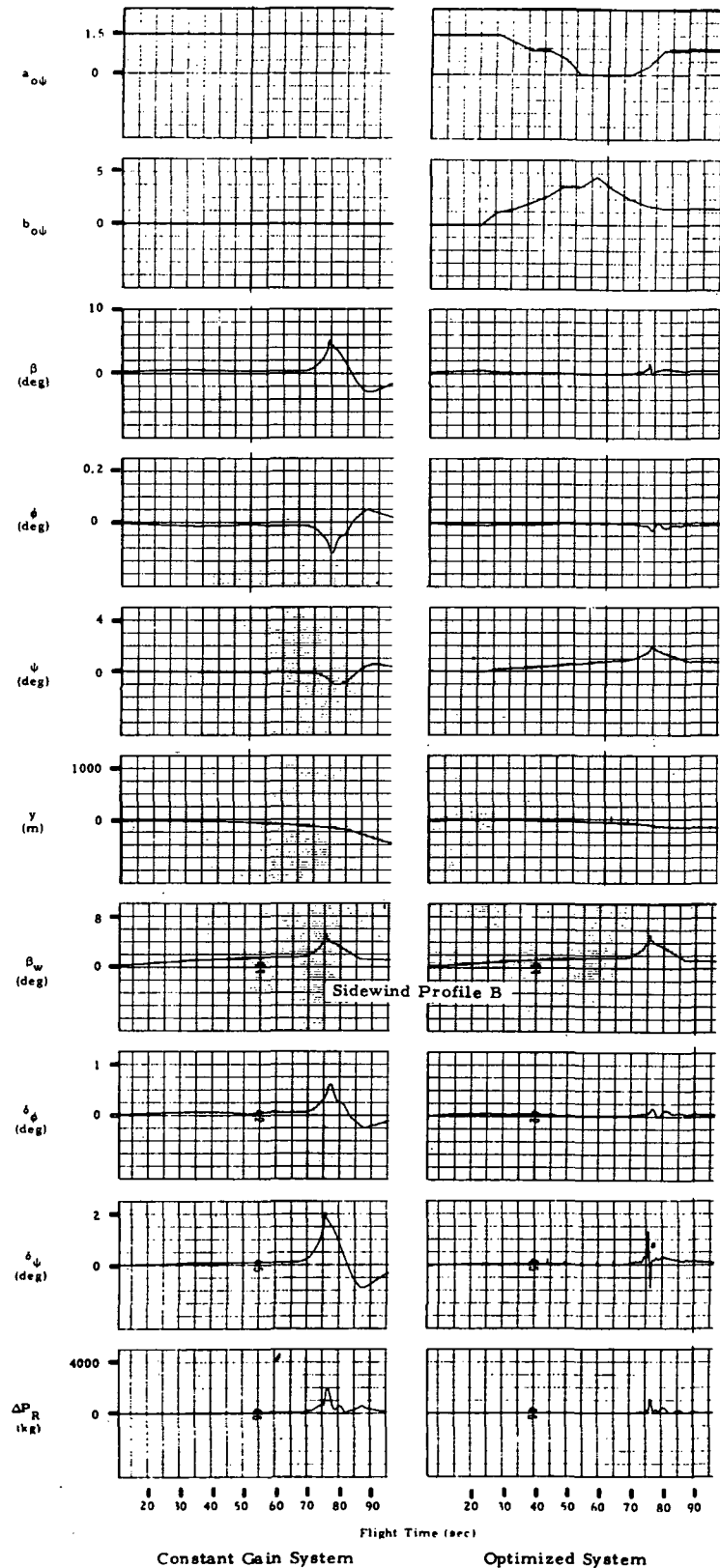


Fig. 3-16 - Performance of Constant Gain and Optimized Gain Systems of Fig. 3-15 Subjected to Sidewind Disturbance B.

lateral drift (y). Again, as in previous results, the $(a_{0\psi})$ schedule follows the classical load relief solution of approaching zero during the region of peak winds. The resolution of the strip charts fail to show that in reality $(a_{0\psi})$ goes slightly negative (≈ -0.03).

The performance of the vehicle may be described as slightly yawing into the wind while maintaining near zero roll and sideslip. An analysis of the interface loading equations also verifies these results in that roll perturbations are the predominant terms causing structural loads at the booster/orbiter rear interface connection. Yaw perturbations contribute insignificantly to the structural loads. The only adverse result noted is the rapid transients of the yaw engine gimbaling (δ_{ψ}). This transient occurs in response to the peak gust. During the studies it was necessary to increase yaw rate feedback gain from 0.5 to 3.0 sec to maintain closed-loop stability during the peak gust. Further studies would be required to reduce these undesirably high gimbal angle rates.

3.6 EFFECTS OF WIND UNCERTAINTIES ON THE OPTIMIZED CONTROL SYSTEM

One of the major advantages of the present hybrid optimization technique is the capability to use more than one flight condition as basis for the optimal design. In the shuttle design study, a pair of adverse wind disturbances were selected to represent two likely flight conditions during optimization, thus reducing the sensitivity to wind uncertainties during launch.

The last part of the study was aimed at determining by simulations to what extent this design objective has been achieved and to gain more experience in selecting representative design wind profiles for best statistical response characteristics.

This wind sensitivity study was performed in the following way: Space shuttle ascent was simulated with the control system using the time-varying

pitch gain schedules optimized for two severe adverse headwinds as presented in Section 3.4 and the time-varying yaw gain schedules which were optimized for two severe adverse 90° -sidewind disturbances of Section 3.5. The most severe of the two design wind profiles (Wind A) was chosen, and its direction was systematically varied between 0 and 90 degrees to the vehicle's launch and pitch plane. Since structural loads at the booster/orbiter interface had been found to affect vehicle weight and payload capability the strongest, peak structural loads $R_{r_{max}}$ in the high dynamic pressure region ($50 \leq t \leq 70$ sec) are plotted as a function of wind direction in Fig. 3-17

For comparison purposes, the corresponding loads for a constant gain control system are also plotted.

It is readily seen that sidewind disturbances are most critical for the structural design. The curves also show that the optimized system is not very sensitive to wind directions that differ from the design cases (0 deg for pitch controller, 90 deg for yaw controller). Thus the design objective of reducing the sensitivity to wind uncertainties has been achieved as far as wind orientation is concerned. Time did not allow a study of the sensitivity to wind profiles different from the two adverse design cases.

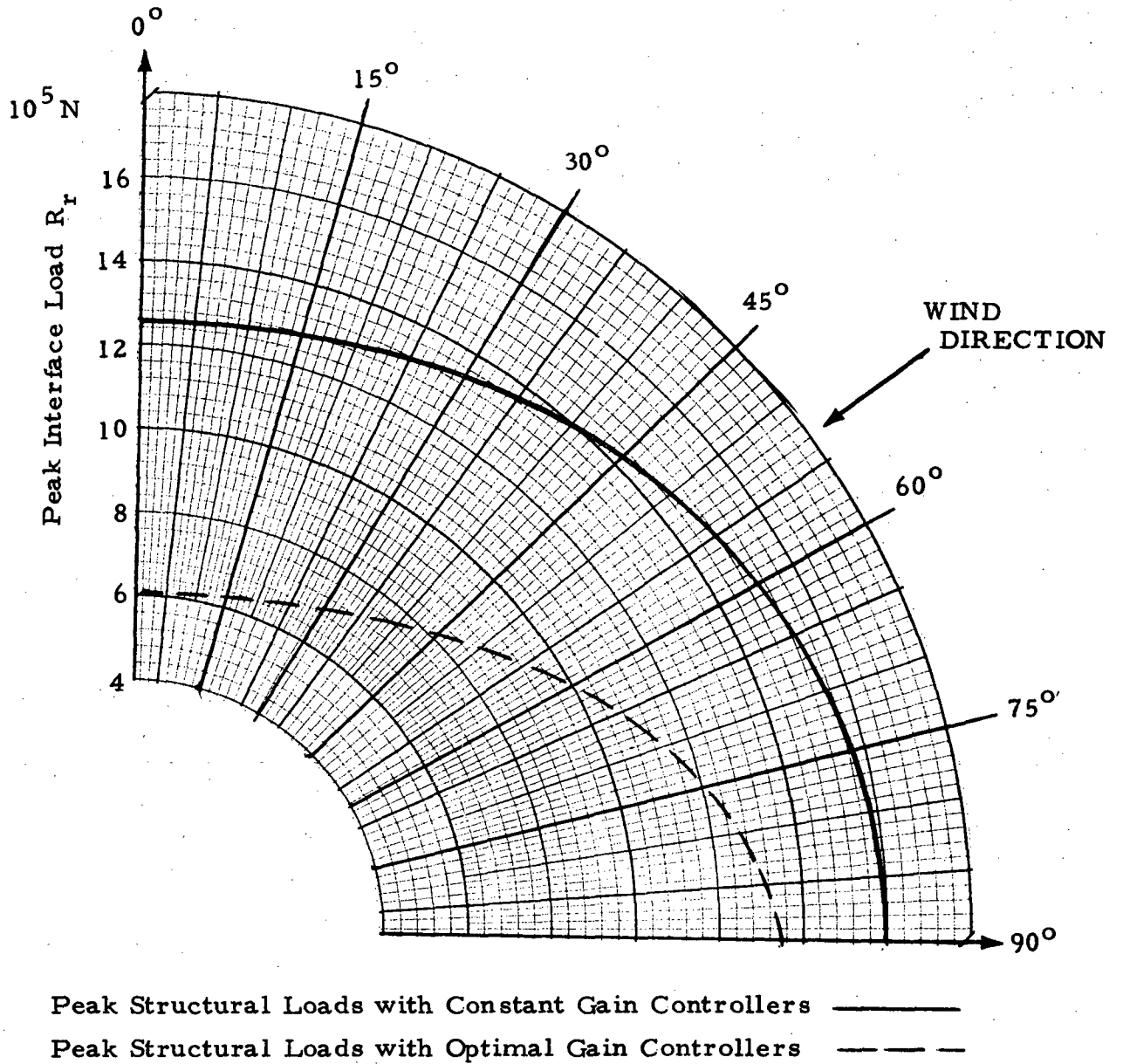


Fig. 3-17 - Peak Structural Loads in the High- q Region ($50 \leq t \leq 70$ sec) as a Function of Wind Direction, Constant Gain Controllers and Optimized Time-Varying Pitch and Yaw Gain Schedules. Wind disturbance (Case A) has maximum shear and superimposed gust at max. αq .

Section 4

CONCLUSIONS AND RECOMMENDATIONS

By combining realistic simulations of vehicle and control system dynamics with an iterative gradient minimization scheme for near-optimal adjustment of time-varying control gain schedules, a practical design tool has been obtained which enables the designer to formulate the design objectives in meaningful engineering terms. Control system design for maximum load relief and design for maximum payload in orbit demonstrate versatility and practical features of the technique. As illustrated by the example of payload-optimal shuttle controller design, this approach requires close cooperation and cross talk between engineers of various fields, dynamics and control, structures, aerodynamics, trajectory optimization and guidance, to provide the necessary data for performance evaluation. The optimal controller designs evolving from such a broad multi-disciplinary effort then account for all the major and often conflicting systems aspects early in the design. In the development of a complex transportation system such as the space shuttle, extensive use of this tool can contribute to a more economical design due to this total systems approach practiced at an early development stage.

Various peripheral computer programs have been developed or brought to operational status during this study for quick reduction of vehicle and trajectory data into suitable form for hybrid simulation, and digital simulation for hybrid computer for analysis and checkout, weight estimation of critical structural subsystems, and for dynamic simulation of complex structural loads during 6-DOF vehicle motion.

These service programs have been kept as general as practical to be applicable to a wide class of shuttle configurations. Future application to

the new low-cost space shuttle concepts will be possible with modest program modifications.

The capability of this optimization tool to reduce the sensitivity to uncertain flight conditions has been demonstrated for assumed wind uncertainties. Certain failure modes during ascent (engine-out, abort separation during high dynamic pressure) represent additional uncertainties which a well-designed flight control system must be capable of handling. An attractive approach would be to optimally design the control system for nominal flight with one or several failure modes representing likely alternate flight conditions to be controllable at some acceptable loss in optimality. This and various related design problems are readily amenable to computerized solution by the present hybrid optimization technique.

Section 5

REFERENCES

1. Trautwein, W., and C. L. Connor, "Hybrid Computer Solutions for Optimal Control of Time-Varying Systems with Parameter Uncertainties," Proceedings, Fall Joint Computer Conf., Houston, Texas, 1970, pp. 135-142.
2. Fletcher, R., and M. J. D. Powell, "A Rapidly Convergent Descent Method for Minimization," Computer J., Vol. 6, 1963.
3. Ryan, R. S., and D. V. Mowery, "A Look at Control Law Influences on the Rigid Body Bending Moments for Boost Vehicles with Various Degrees of Aerodynamic Stability," AIAA paper, 71-918, August 1971.
4. "Space Shuttle Program Phase B Final Report - Technical Summary," Report MDC E0308 Part II, McDonnell Douglas Corp., St. Louis, Mo., 15 March 1971.
5. Trautwein, W., and J. G. Tuck, "Control System Optimization for Saturn V Launch Vehicles Using Gradient Techniques," Final Report, LMSC-HREC A791836, Lockheed Missiles & Space Co., Huntsville, Ala., October 1968.
6. Daniels, Glenn E. (Editor), "Terrestrial Environment (Climatic) Criteria Guidelines for Use in Space Vehicle Development, 1969 Revision," NASA TM X-53872, Marshall Space Flight Center, 15 March 1970.
7. Sharp, J. B., L. W. Foster and D. R. Kennemur, "Intermediate-21 Load Relief Attitude Control," M-725-895, Northrop Corp., Huntsville, Ala., March 1971.
8. Livingston, John M., Jr., and Jerome R. Redus, "Load-Reducing Flight Control Systems for the Saturn V with Various Payloads," NASA-Marshall Space Flight Center, Huntsville, Ala., AIAA Paper No. 68-843.
9. Anderson, H. A., "Booster Hydrogen Tank Cylinder Design," Design Note B-WEST-STR-3, McDonnell Douglas Corp., St. Louis, Mo., 16 September 1970.
10. Wright, F. M., "Minimum Weight Design of Flanged Isogrid Cylinders in Compression," Design Note B-WEST-STR-7, McDonnell Douglas Corp., St. Louis, Mo., 11 September 1970.

11. Garrison, G. S., and D. R. Kilpatrick, "Shuttle Exchange Ratio Study Using the McDonnell Douglas High Crossrange Canard Configuration 20," M-796-945, Northrop Corp., May 1971.
12. Ryan, R. S., D. L. Bacchus, C. E. Hall, and D. V. Mowery, "Space Shuttle Engine Gimbal Requirements," IN-AERO-71-1, MSFC Aero-Astroynamics Laboratory, January 1971.
13. Trautwein, W., C. L. Connor, and J. M. Livingston, "Computerized Optimal Control System Design for Reusable and Expendable Boost Vehicles," AIAA 10th Aerospace Sciences Meeting, AIAA Paper No. 72-98, San Diego, Calif., 17 January 1972.